Document Number**:** H2020-ICT-52/RISE-6G/D5.2

Project Name:
Reconfigurable **I**ntelligent **S**ustainable **E**nvironments for **6G** Wireless Networks
(RISE-6G)

Deliverable D5.2

Algorithms for RIS-based Localisation and Sensing (Intermediary Specifications)

Deliverable D5.2
Algorithms for RIS-based Localisation and Sensing (Intermediary Specifications)

Project Number:	H2020-ICT-52 / 101017011
Project Name:	**R**econfigurable **I**ntelligent **S**ustainable **E**nvironments for **6G** Wireless Networks

Document Number:	H2020-ICT-52/RISE-6G/D5.2
Document Title:	Algorithms for RIS-based Localisation and Sensing (Intermediary Specifications)
Editor(s):	Radoslaw Kotaba (AAU)
Authors:	Vincenzo Sciancalepore (NEC), Francesco Devoti (NEC), Georgios Alexandropoulos (NKUA), Ioanna Vinieratou (NKUA), Moustafa Rahal (CEA), Benoit Denis (CEA), Paolo Di Lorenzo (CNIT), Stefania Sardellitti (CNIT), Henk Wymeersch (CHA), Kamran Keykhosravi (CHA), Musa Furkan Keskin (CHA), Hyowon Kim (CHA), Kimmo Kansanen (AAU)
Dissemination Level:	PU
Contractual Date of Delivery:	30/06/2022
Security:	Public
Status:	Final
Version:	1.0
File Name:	RISE-6G_WP5_D5.2_final.docx

Abstract

This deliverable summarizes the work on flexible estimation and detection algorithms for RIS-based localisation, mapping and sensing performed within work package 5 "RIS for Enhanced Localisation and Sensing" of the RISE-6G project.

Keywords

Beyond-5G; 6G; RIS; Localisation; Sensing; Connectivity

Contents

List of Figures

List of Tables

List of Acronyms

5G-NR	5th Generation - New Radio
5G-PPP	5G infrastructure Public Private Partnership
AMF	Access and Mobility management Function
AoA	Angle of Arrival
AoD	Angle of Departure
AML	Approximate maximum likelihood
AMML	Approximate mismatched maximum likelihood
BP	Belied Propagation
BS	Base Station
CAPEX	CAPital EXpenditure
CDF	Cumulative Density Function
CRB	Cramér-Rao bound
CSI	Channel state information
DAE	Denoising Autoencoder
DL	Downlink
DL-DoD	Downlink Direction of Departure
DL-TDoA	Downlink Time Difference of Arrival
DoA	Direction of Arrival
DoD	Direction of Departure
(E)KF	(Extended) Kalman Filter
EM	Electromagnetic
EMF	Electro Magnetic Field
FF	Far-field
FFT	Fast Fourier Transform
FIM	Fisher information matrix
FMCW	Frequency Modulated Continuous Wave
GDoP	Geometric Dilution of Precision
GLRT	Generalized Likelihood Ratio
GOSPA	Generalized Optimal Sub-pattern Assignment
IFFT	Inverse Fast Fourier Transform
KPI	Key-Performance Indicator
LB-AoI	Localisation Boosted - Area of Influence
LE-AoI	Localisation Enabled - Area of Influence
LMF	Location Management Function
LOF	Local-Outlier-Factor
LoS	Line-of-Sight
LTE	Long Term Evolution
MAP	Maximum A Posteriori
MC	Multicarrier
MIMO	Multiple Inputs Multiple Outputs
ML	Maximum Likelihood
MMSE	Minimum Mean Squared Error
MP	Message Passing
MCRB	Miss-specified Cramer Rao Bound
MTBF	Mean Time Between Failures
NF	Near-field
NLoS	Non-line-of-sight
NVAA	Non-Value-Added Activities
OFDM	Orthogonal Frequency Division Multiplexing
OMP	Orthogonal Matching Pursuit
OPEX	OPerating EXpenditure
PDF	Probability Density Function
PEB	Position error bound
PF	Particle Filter
RF	Radio Frequency

R-RIS	Reflective RIS
RT-RIS	Reflective-transmission RIS
RIS	Reconfigurable Intelligent
RISC	RIS controller
RISO	RIS orchestrator
RMSE	Root Mean Square Error
RSSI	Received Signal Strength Indicator
RTT	Round Trip Time
RT-ToF	Round Trip – Time of Flight
Rx	Receiver
SCA	Successive Convex Approximation
SDR	Software Defined Radio
SISO	Single Input Single Output
SLAM	Simultaneous Localisation and Mapping
SP	Scattering Point
SNR	Signal-to-noise ratio
TDoA	Time Difference of Arrival
ToA	Time of Arrival
Tx	Transmitter
UAV	Unmanned Aerial Vehicle
UE	User Equipment
UTDoA	Uplink Time Difference of Arrival
UL	Uplink
UL-DoA	Uplink Direction of Arrival
UL-TDoA	Uplink Time Difference of Arrival
VA	Virtual Anchor
VEB	Velocity Error Bound
WB	Wideband
WFL	Wireless Fingerprinting Localisation
(W)LS	(Weighted) Least Squares

1   Introduction

The RISE-6G project is one of the 5G infrastructure Public Private Partnership (5G-PPP) projects under the European Commission's Horizon 2020 framework. The focus of the project is to design, prototype, and trial radical technological advances based on reconfigurable intelligent surfaces (RISs) to forge a new generation of dynamically programmable wireless propagation environments. RISs will both enable and boost connectivity, localisation, and sensing performance, as well as adapt to dynamic requirements on electromagnetic field emissions, energy efficiency, and secrecy.

Within RISE-6G, work package 5 (WP5) considers exploiting RIS for improved localisation, sensing and mapping performances. The aim of WP5 is two-fold: (i) to develop localisation-oriented network architecture for RIS deployment and profile control to optimise the aforementioned features' key performance indicators (KPIs); (ii) to develop and evaluate detection and estimation algorithms that enable RIS-based localisation and sensing, for localising connected wireless devices, building dynamic environments and radio maps, as well as passively sensing physical features.

1.1   Deliverable objectives

This document provides the intermediate results related to Task 5.2 (objective (ii) above) from WP5 and contains a summary of relevant contributions developed within that work package.

Given the a priori RIS locations and orientations, as well as selected architectures and deployment strategies from T5.1 (and corresponding deliverable D5.1 [RISED51]), it addresses the following research items as outlined in the project description of action:

- **Estimation of location-dependent RIS-enabled multipath parameters**: design of suitable estimators for multipath delays/power/angles of departure and arrival, and Doppler shifts. Blind and semi-blind approaches, in conjunction with advanced beam-training strategies (e.g., based on prior mobile location information), are considered under partial and/or imperfect prior Channel State Information (CSI) of end-to-end and side RIS channels, in both initial and steady-state (i.e., tracking) regimes.

- **Estimation of active UEs and passive objects:** using various approaches that can either exploit the location-dependent channel parameters and radio metrics obtained with techniques described above, or by performing positioning directly out of the received signals, with no intermediary channel estimation step

- **RIS-enabled SLAM**: development of low-complexity algorithms that can solve both simultaneous localisation and mapping (SLAM) and opportunistic sensing problems, while relying on RIS-enabled communication links between the Base Station (BS) and User Equipments (UEs). Solutions that offer high nominal accuracy and resilience against generalized Non Line of Sight (NLoS) conditions, mitigate RIS-induced multipath interference are sought after.

- **Spectrum sensing, Radio Frequency (RF) mapping and fingerprinting localisation**: Leveraging the deployment of a large number of RISs, sensing of the wireless activity can be performed with cm-level resolution. Furthermore, it enables wireless fingerprinting localisation (WFL) based on existing network infrastructure such as WiFi or cellular networks, which represents an effective yet practical (in terms of extra hardware deployment) technique.

The results and algorithms presented here serve as an input to WP6, where localization and sensing information is used to control EMF exposure and to WP7, where a subset of methods will be implemented and used in proof-of-concept validations relying on real hardware.

1.2   Deliverable structure

The rest of the document is structured as follows.

In Section 2 the basics of localisation and sensing are provided, contrasting conventional approaches that do not rely on RIS(s) with new techniques leveraging the presence of latter.

The relevant KPIs are described in Section 3, along with methods for evaluating them.

Section 4 focuses on the estimation of channel parameters from a localisation and sensing standpoint. Four different approaches developed within this project are detailed in corresponding subsections.

In Section 5, six techniques for estimation of active UEs locations are presented for various BS-RIS-UE deployment scenarios, RIS operating modes and propagation conditions.

Complimentarily to Section 5, in Section 6 methods of detection of the passive (uncontrolled) objects are provided, as well as techniques to perform simultaneous localisation and mapping (SLAM) in the presence of RIS(s).

Section 7 details another localisation paradigm based on wireless fingerprinting via spectrum sensing and RF mapping.

The interactions with work package 7 (WP7), including practical considerations and potential proof of concepts implementations of the algorithms presented earlier are detailed in Section 8.

Lastly, Section 9 offers some concluding remarks for this deliverable.

2   Localisation and Sensing

The purpose of this section is to provide a brief overview of the principles of radio localisation and sensing, with an emphasis on cellular approaches. Then the general use of reconfigurable intelligent surfaces (RISs) in the context of localisation and sensing will be detailed.
The issues related to the architectures and control methods are discussed in a separate deliverable D5.1 [RISED51].

2.1   Foundations of localisation

In the context of radio systems, localisation (synonym: positioning) is the process of determining the 2D or 3D location of a connected device (a user equipment (UE)), based on uplink (UL) or downlink (DL) measurements with respect to several base stations (BSs) [PRL+18]. The measurements are performed based on the reception of dedicated pilot signals and can be of the forms described in Table 2-1. Observe that a combination of angle and delay measurements can be used for UE localisation and that different measurement combinations put different requirements on both the number of BSs as well as on their mutual synchronization [KDA+22]. For this latter reason, pure ToA measurements with an UE synchronized to a BS is impractical in real scenarios, since even small synchronization errors lead to large localisation errors (e.g., 10 ns clock error corresponds to 3 meters error). Examples of two different measurement for localisation are shown in Figure 2-1.

Table 2-1. Localisation measurements and requirements for 3D positioning.

Measurement	UL or DL	Number of BSs needed	Comment
Time-of-arrival (ToA) of the first path	Either	3	BSs should be synchronized with the UE
Time-difference-of-arrival (TDoA), derived from several ToA measurements	Either	4	BSs should be mutually synchronized
Round-trip-time (RTT), derived from several ToA measurements	Both	3	No synchronization needed
Angle-of-arrival (AoA)	UL	2	Requires planar arrays at each BS
Angle-of-departure (AoD)	DL	2	Requires planar arrays at each BS
TDoA+UL-AoA	UL	2	BSs should be mutually synchronized
RTT+ UL-AoA	Both	1	No synchronization needed
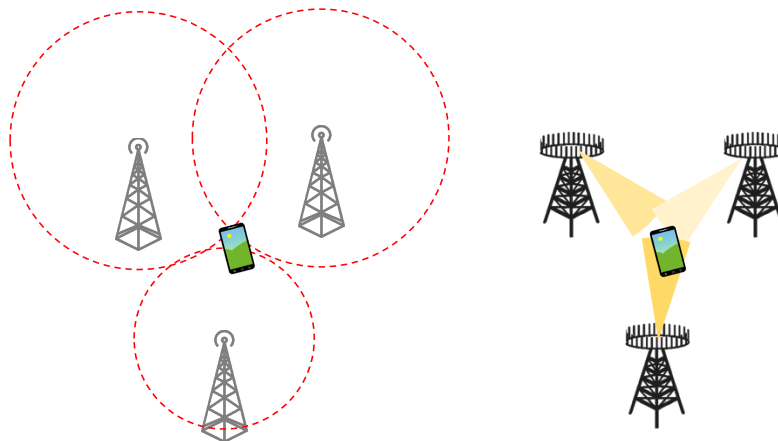
Figure 2-1. Example of RTT-based localisation (left), constraining the UE on the intersection of circles (2D) or spheres (3D). On the right, an example of localisation based on DL-AoD measurements, constraining the user within a sector of each BS.

The pilots used for localisation are tailored in time, frequency, and space. In time-frequency, so-called comb signals are used, which occupy the entire signal bandwidth while allowing orthogonality across BSs [3GPP10]. In space, the time-frequency signals are repeated for different directional beams at the BS, while providing angle measurements (AoA in UL or AoD in DL). The quality of the ToA and AoA/AoD measurements depends on several factors [WLW+18]:

- **Bandwidth:** the amount of available bandwidth is directly related to delay resolution and thus to multipath suppression (in particular, two paths can be resolved if their delay difference is at least 1 over the bandwidth). If strong signal paths are present, say, 10 meters after the direct path, then a bandwidth of around 30 MHz is needed to resolve this secondary path. For that reason, a large bandwidth is important for accurate localisation in cluttered environments.

- **Transmission power:** the accuracy of delay and angle measurements depends on the received signal-to-noise ratio (SNR), which is itself proportional to the transmission power. Hence, higher transmit powers lead to more accurate localisation, provided multipath can be resolved. Since localisation depends on pilot signals, an increase in SNR can also be achieved through longer transmission times.

- **Number of antennas:** similar to bandwidth being related to delay resolution, so is the number of antennas proportional to angle resolution (the relation for a linear array is that two paths with angle difference (in radians) beyond 2/(number of antennas) can be resolved). Hence, a larger array of half-wavelength spaced elements leads to improved angular resolution, which can be traded off against delay resolution.

- **Signal processing and hardware limitation:** depending on the computational capacity and knowledge regarding the utilised beams, the delay and angle estimation performance can be improved. Moreover, hardware and calibration errors (e.g., synchronisation errors) significantly affect localisation performance, leading possibly to a significant gap between theory and practice.

2.2 Foundations of sensing

In contrast to localisation, 3GPP has until now not offered any support for radar-like sensing.

Such sensing is conventionally broken down as [WSD+21]:

- **Monostatic sensing:** a transmitter (Tx) and a receiver (Rx) are co-located and share a common clock. The Tx emits a waveform, known to the Rx. The Rx processes the backscattered waveform to detect the presence of targets (static or dynamic object), as well as their distance, bearing, and velocity. Such type of radar sensing is commonly employed in automotive radar, and requires dedicated waveforms, shaped in time and frequency (e.g., frequency modulated continuous wave (FMCW) [LLH+16] [SFS+18]) with orthogonality across transmit antennas, to provide a large virtual aperture. FMCW-type waveforms have a constant envelope, making them hardware-friendly. In the context of communication systems, standard data-bearing signals can be used (e.g., orthogonal frequency division multiplexing (OFDM)) [CKA+20]. Monostatic sensing requires a full-duplex receiver.

- **Bistatic sensing:** in this mode, Tx and Rx are not co-located and do not share a common clock. Pilot signals are emitted by the Tx and the backscattered signal is processed by the Rx. The lack of synchronization requires a clock reference, which can be offered by the direct path between Tx and Rx.

- **Multistatic sensing:** this is a generalization of bistatic sensing with several Rx. The information for the different Rxs must be fused to provide an overall picture of the detected objects. The larger number of Rxs allows for higher resolution, due to the increased aperture, provided the Rxs are synchronized.

The discussion related to delay and angle resolution, as well as signal processing and hardware limitations from Section 2.1 is still relevant. In terms of power, it is important to note that sensing is subject to more severe path loss than localisation, as the signal scatters from objects before reaching the Rx.

2.3 RIS in localisation and sensing

RISs have potential to improve localisation and sensing performance, when added to conventional deployments [WHD+20]. This is referred to as 'boosting'. In addition, RIS also have the potential to provide location estimates to UEs when conventional deployments fail. This is referred to as 'enabling'.
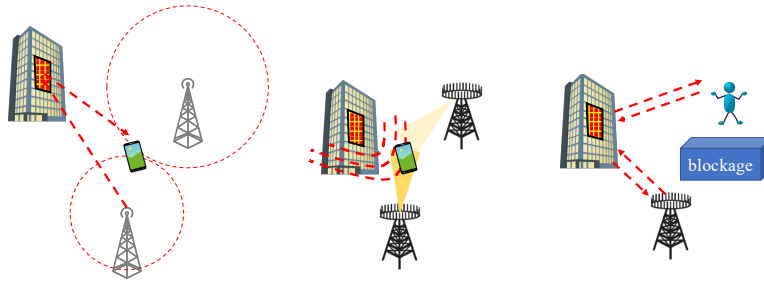
Figure 2-2. Examples of use of RIS in localisation: a new signal path via a RIS and a new reference by the RIS (left); large RIS provides wavefront curvature for localisation measurements (middle); a RIS provides a signal path to avoid signal blockage in mono-static sensing.

In wireless systems, RISs can boost or enable user localisation by providing the following features (see Figure 2-2):

1. **New signal path**: The reflected signal from the RIS provides the Rx with an additional signal path whose parameters can be estimated and used for localisation. Compared to other multipath generated by the scatterers, the path from the RIS is stronger due to the multitude of RIS elements and beamforming gain.

2. **New location references**: RISs, when used as a part of wireless infrastructure, have a fixed location and orientation. Therefore, they provide a location reference that can be used to estimate the unknown location of the user. This separates RISs from scatterers in the environment as the location of the scatterers are often unknown.

3. **Near-field (NF) measurements:** Since the dimensions of RISs are much larger than the conventional planar arrays used in Multiple Inputs Multiple Outputs (MIMO) systems, and they can be installed close to the user site, it is probable that the user falls within the near-field of the RIS [DNA+21]. In the near-field, one can also use the phase of the received signal to estimate directly the location of the user.

In Table 2-2, we present some of the scenarios where the user localisation in 3D is possible for wireless systems equipped with RISs. Here we only consider single-antenna BSs.

Table 2-2 RIS Localisation measurements and requirements for 3D positioning.

Measurement	UL or DL	# BSs	#RISs	Comment
ToA + AoD	Both	0	1	No synchronisation needed
TDoA + AoD	Either	1	1	No synchronisation needed
AoD	Either	1	2	No synchronisation needed

3   Key performance indicators, methods, and evaluation

3.1   Localisation and sensing performance metrics

In this subsection, we recall generic metrics and indicators initially introduced in Deliverable 2.4 [RISED2.4] that are used to assess the performance of RIS-based localisation and sensing. As already suggested above, the *sensing* functionality shall be intended here as the *localisation of passive entities* (i.e., non-connected objects or non-cooperative devices), in contrast to the active localisation of connected devices, which is simply depicted as *localisation*. Accordingly, all the localisation-oriented metrics detailed below would still hold for the evaluation of sensing performances. Additional metrics can be found in the literature, e.g., [ZGL19].

3.1.1 Localisation accuracy

Accuracy is fundamentally determined by the statistics of the 3D localisation error $\mathbf{e} = \mathbf{x} - \hat{\mathbf{x}}$, which represents the deviation of an estimate $\hat{\mathbf{x}}$ from a Ground-Truth location $\mathbf{x}$. This error is usually seen as a random variable comprising both horizontal (XY) and vertical (Z) error components. Accuracy is arguably the most relevant and definitive metric to characterize any localisation method, as it intrinsically accounts for several -and likely combined- factors, such as received signal-to-noise-ratio (SNR), resolution capabilities (i.e., the separability of correlated received radio signals) and state identifiability (i.e., the existence of a continuous or discrete set of possible solutions, depending on both connectivity conditions and network deployment geometry). Relevant statistics characterizing the 3D or 2D localisation errors include e.g.,

- **Mean Square Error (MSE):** $\mathbb{E}[\mathbf{e}^T \mathbf{e}]$;
- **Root MSE (RMSE):** $\sqrt{\mathbb{E}[\mathbf{e}^T \mathbf{e}]}$;
- **Accuracy (with confidence level α):** $e: p(\|\mathbf{e}\| < e) = \alpha$;
- **Horizontal accuracy (with confidence level α):** $e: p(\|\mathbf{e}_{1:2}\| < e) = \alpha$;
- **Vertical accuracy (with confidence level):** $e: p(|e_3| < e) = \alpha$.

The evaluation of accuracy levels typically relies on the cumulative distribution function (CDF) of the localisation estimation error, which can reflect more accurately effects such as heavy-tailed/asymmetric localisation error distributions, beyond more "compact" indicators such as MSE. Alternative metrics such as the circular error probability (CEP) or the hit target radius (HTR) can also be considered. CEP is defined as the probability for a location estimate to fall into a circle (resp. sphere) of radius R centred around the ground-truth location in 2D (resp. 3D). HTR corresponds to CEP equal to 50%.

3.1.2 Localisation-related delays

As localisation is often time-sensitive and sometimes safety-critical, there are also specific localisation-related delay metrics that impact the reactivity of the localisation system, as well as its capability to cope with mobility (typically from a tracking standpoint in the steady state regime), namely.

- **First time to fix**: time until the system provides the first location estimate.
- **Localisation latency:** time between a positioning request and the position being available.
- **Update rate**: time between successive position estimates.

3.1.3 Localisation integrity

In certain critical applications, the localisation error cannot exceed certain safe thresholds and the localisation service must be available without interruption. Relevant metrics in this regard are:

- **Reliability:** measured by mean-time between failures (MTBF) or duration of the time the service is available.
- **Availability:** fraction of the time the service is available.

High reliability means high availability, but not the other way around. Hence, a system that is down (i) every other minute for 1 minute or (ii) every other hour for 1 hour has the same availability, but very different reliability.

Table 3-1 Main performance metrics.

Metric	Unit	Example	Comments
Location accuracy	Meter	1 meter accuracy with 95% confidence	Accounts for both biases and variance (precision and accuracy).
Latency	Seconds	10 ms	Includes control and signalling overhead, signal transmission time, and signal processing.
Update rate	Hertz	1 Hz	Bounded by the latency.
Reliability	Seconds	A MTBF of 50 hours means that the system on average works for 50 hours until a failure occurs	Depends mainly on uptime of base stations and user devices.
Availability	% or fraction of time	99.99% or 23.9976 hours in 24 hours.	Depends also on deployments, and uncontrolled factors (e.g., environment).

3.2 Methods and evaluation

Based on the previous metrics and indicators, the chosen methodology to practically assess the performance of the proposed RIS control mechanisms and/or RIS-enabled system architecture in the RISE-6G project is based on both numerical simulations (incl. theoretical performance bounds evaluations) and real experimental data (i.e., either by emulating the system offline, or through real-time demonstrations). Although we develop both aspects in this subsection for the sake of completeness, the focus of this deliverable is put on the former simulation-based evaluations.

3.2.1 Theoretical bounds

First, theoretical performance bounds are used to provide strong guarantees on both the optimality and the reliability of the proposed RIS-enabled localisation solutions. Typically, the position error bound (PEB) is a theoretical tool accounting for the best localisation accuracy achievable by any unbiased estimator, assuming a priori statistics for the measured radio signals (or for radio metrics estimated out of received signals) used as observations, as well as the knowledge of user's and BSs' locations. The PEB is defined from the Fisher information matrix $\mathbf{J}$, which represents a theoretical lower bound on the error covariance, as follows:

$$\mathbf{J}^{-1}(\mathbf{x}) \preccurlyeq \mathbb{E}[(\mathbf{x} - \hat{\mathbf{x}})(\mathbf{x} - \hat{\mathbf{x}})^{\mathbf{T}}].$$

The PEB (expressed in meters) at a location $\mathbf{x}$ is then calculated as

$$\mathbf{PEB}(\mathbf{x}) = \sqrt{\mathbf{trace}(\mathbf{J}^{-1}(\mathbf{x}))} \leq \sqrt{\mathbb{E}[\|\mathbf{x} - \hat{\mathbf{x}}\|^2]}.$$

Given any concrete scenario under test (i.e., simulated, or experimental), the PEB can hence be numerically evaluated as a function of key system parameters (e.g., SNR per radio link, operating frequency, bandwidth, etc.) and the true locations of all the physical entities involved in the localisation problem (incl. that of the user or objects to be positioned).
Note that there exists a variety of bounds to the achievable accuracy apart from the well-known Cramer-Rao bound described above, such as the Weiss-Weinstein bound or the Ziv-Zakaï bound, which are typically more suitable at low SNR regimes.

Finally, to assess uniquely the effect of network deployment geometry (i.e., user's relative position with respect to BSs) regardless of SNR conditions, one can evaluate the geometric dilution of precision (GDoP) in 2D or 3D, which is somehow already integrated by default in the PEB calculation.

3.2.2 Simulations

In simulation-based evaluations, the evaluation of accuracy levels practically relies on the empirical CDF of the localisation estimation error, which is obtained over multiple simulation trials while introducing randomness between these successive trials (e.g., in terms of noise realizations and/or tested positions, etc.), depending on the considered scenario. This empirical CDF is used in practice to characterize characteristic error values. Such critical values include for instance the median error at 50% of the CDF, or so-called "worst case" localisation error at arbitrary high CDF values, typically 90% or 99%, i.e., the critical error value such that 90% or 99% of the localisation errors (over all simulation trials) have a smaller magnitude.

Ideally, the tested localisation methods themselves are also expected to provide a localisation error indicator (e.g., a 90% confidence ellipsoid). The size of this ellipsoid is then interpreted as a reliable measure of the accuracy, as perceived internally by the algorithm (and given that no overconfidence issue has been spotted within the estimation process).

A priori, localisation-related delays are not trivial to assess in absolute values through simulations, given the typically high levels of system abstraction of signal-oriented simulation tools. However, impacting aspects such as overhead or frame durations can at least be covered in more protocol-oriented simulations.

3.2.3 Experiments

Evaluations based on experimental data are typically split in two categories depending on the available hardware, namely *offline system emulations* (based on e.g., pieces of metrology equipment such as channel sounders) and quasi *real-time trials* (based on e.g., integrated devices, as close as possible to commercial devices). In both categories, the measurement of the localisation accuracy requires a side **ground-truth referencing system**, whose uncertainty should be at least several orders of magnitude below that of the system under test. This ground-truth system is particularly challenging in dynamic indoor scenarios, so that simplified approaches are often applied (typically, projecting time-stamped localisation estimates onto piece-wise segments of the followed path), at the price of approximations. In static scenarios (i.e., freezing a deployment configuration and for a given position under test), just like in simulation-based evaluations, the accuracy levels can be simply assessed with the empirical CDF of the localisation estimation error, which is obtained over a sequence of successive measurements.

As for localisation-related delays, they can be measured at the mobile UE or network side, depending on (i) where the location computation takes place, (ii) which system entity requests the location information and (iii) where the latter information must be ultimately issued. The localisation application itself should also provide timestamps of when the measurements were taken, when the location was computed, and when the location was provided to the application.

As the localisation application is supposed to provide an evaluation of the localisation uncertainty (e.g., 90% confidence ellipses or covariances), integrity monitoring (incl. fault detection and exclusion) can be performed externally to the localisation application itself. Practically, one can simply measure how often the actual localisation error exceeds the uncertainty values indicated by the localisation error covariances (i.e., timewise or per attempt), that is, the fraction of instances when the actual error is outside the confidence levels provided by the application's uncertainty estimates.

4 Estimation of location-dependent multipath parameters in RISE channels

4.1 Motivations and challenges

Localisation is often performed as a two-step process, consisting first of a channel parameter estimation routine, which determines the number of resolvable signal paths, as well as the associated ToA, AoA, and AoD. Secondly, the Line of Sight (LoS) path (e.g., with shortest delay or largest channel gain) is used for localisation, while remaining paths are either discarded or used for mapping. There is a large body of literature on such parametric channel estimation, including ESPRIT [RHD14], generalized approximate message passing [BSY19], orthogonal matching pursuit [SGD+17] and RIMAX/SAGE [TLR04]. Note that channel parameter estimation is distinct from (unstructured) channel estimation [BG06], which aim to determine the complete channel matrix or vector, based on pilot transmissions. This unstructured channel estimate is usually an input for parametric channel estimation. Unstructured channel estimation is used in the context of localisation for fingerprinting.

The role of RIS in channel parameter estimation can be broken down as follows:

- **A reflective RIS** provides an additional signal path to a receiver. If this path can be resolved from the uncontrolled multipath (possibly including the direct path from transmitter to receiver), the ToA and AoA or AoD from the RIS can be estimated. The resolvability of the path can be ensured (at least for the signal path from RIS to receiver) through dedicated time encoding of the RIS configurations. Then, the receiver can separate this path from all uncontrolled paths and determine the ToA, AoA, or AoD. Moreover, in a multi-RIS context, orthogonal coding by different RIS allows perfect separation of the signal from each RIS at the receiver.

- **A hybrid RIS** acts as a phased array and observes the incoming signal only through its compressed observations, based on the sequence of RIS configurations. The signal from a transmitter to a hybrid RIS when affected by multipath propagation cannot be decomposed in a direct path (transmitter to RIS) and other paths. Hence, more sophisticated methods are needed to determine the ToA and AoA of the direct path.

Ideally, the estimated path parameters should be accompanied with associated uncertainties, prior to performing localisation.

4.2 RISE-6G Contributions

An overview of the different contributions is provided in Table 4-1

Table 4-1 An overview of parameter estimation contributions

Architecture	Cont. #A-1: Far-field ToA and AOD estimation of a signal reflected by a RIS	Cont. #A-2: Far-field ToA and AOD estimation in full-duplex of a signal reflected by a RIS	Cont. #A-3: Near-field ToA and AoD estimation of a signal reflected by a RIS	Cont. #A-4: AOA estimation at a sensing RIS
Nr BS	1	0	1	0
Nr RIS	Multiple	1	1	1
Nr UEs	Multiple	1	1	1
UE Mobility	Stationary	Stationary	Stationary	Stationary
RIS Type	Reflective	Reflective	Reflective	Sensing
Setup				
Uplink/Downlink	Downlink	Uplink	Downlink	Uplink
Indoor/outdoor/UAV	Outdoor	Outdoor	Indoor and outdoor	Indoor and outdoor
Frequency Band	30 GHz	28 GHz	28 GHz	30 GHz
Narrowband/wideband	Wideband	Wideband	Narrowband	Narrowband
Near field/far field	Far field	Far field	Near field	both

LOS/NLOS (BS-RIS-UE)	LOS (Tx-Rx) and NLOS (Tx-RIS-Rx)	LOS (UE-RIS-UE)	NLOS	RIS-UE
Imperfections or other hardware considerations	-	-	Phase-dependent RIS amplitude variations	-
Measurement type	ToA and AoD	ToA and AoD	ToA and AoD	AoA
RIS configuration strategy	Random profile	Directional profile	Random profile	DFT or Random
Who collects measurements	Rx	UE	UE	RIS
Synchronisation	Unsynchronized	-	No	No

4.2.1 Contribution #A-1: Far-field ToA and AOD estimation of a signal reflected by a RIS.

Motivation and context

In this contribution, the aim is to determine the ToA and AoD from a path reflected by a RIS, under the assumption that the AoA at the RIS is known (which is possible when the transmitter and RIS have known location and orientation). An example is shown in Figure 4-1, where a UE observes several paths, including the one reflected by an RIS. The path from the RIS conveys both AoD information as well as ToA information, which will be used for UE localisation [KKS+21] as well as semi-passive RIS localisation in [KKD+21], shown in Figure 4-2. The localisation process will be further elaborated in Section 5.
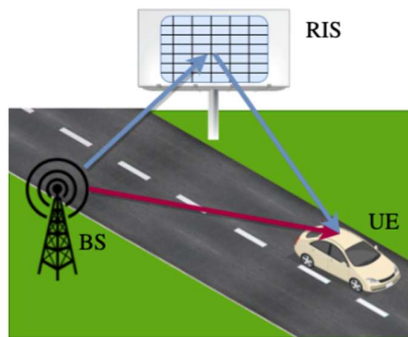
Figure 4-1: User localisation in a SISO system with one RIS. The goal is to estimate the ToA and AoD from the RIS path, as well as the channel parameters of the passive multipath.
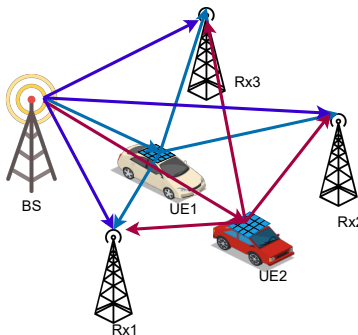
Figure 4-2. RIS localisation based on ToA at several receivers.

The problem is challenging for several reasons:

1. The LoS path and uncontrolled (passive) multipath create interference.

2. The RIS does not process the signal directly, so it is not possible to use standard array processing to estimate the AoD.

Methodology

Each receiver receives signals from a number of paths, these paths can be separated at each receiver via applying a temporal orthogonal code (see [KKD+21]). Therefore, the focus here is only on how to estimate the ToA based on the received signal from a RIS path. For the passive multipath, standard parametric channel estimation routines can be applied, such as ML, SAGE, or ESPRIT.

1. **Finding a coarse estimate of the ToA using FFT operation**: since the structure of the received signal across subcarriers resembles that of the FFT columns, we can use the FFT of the received signal (across subcarriers) to find a coarse estimate of the TOA. This estimation is performed by finding the index of the largest entry of the FFT of the received signal and scaling the index. However, the accuracy of this step is limited by the FFT dimension, and the result should be refined. Note that when single-carrier transmission is used, the ToA cannot be estimated.

2. **Refining the coarse estimation:** In general, to estimate the ToA based on the received signal, one should solve a non-convex optimization problem. This optimization can be solved effectively by performing via a gradient-decent algorithm if the initial point is close to the global optimum. Therefore, here we use the estimate obtained in the first step and use it as the initial point for a quasi-Newton algorithm. Figure 4-3 shows an example of the objective function used for ToA estimation. The coarse estimation is shown by the star and the fine one by the cross.

3. **AoD estimation:** After the ToA is known, its effect can be removed from the observation. The AoD can then be determined by a line search (1D, for linear RIS) or grid search (2D, for planar RIS).
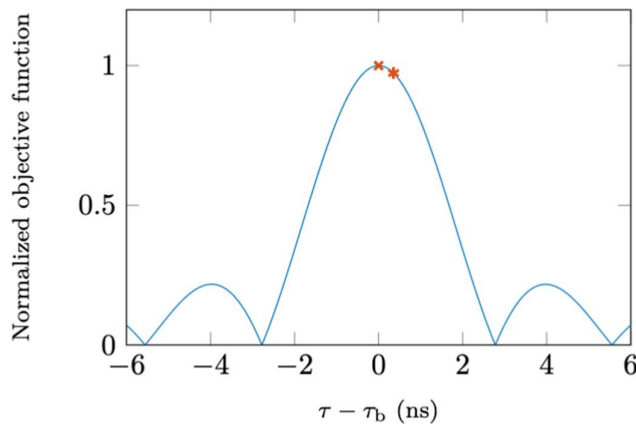
Figure 4-3: An example of a normalized objective function for estimation of ToA. The coarse estimate is shown by a star and the refined one by a cross.

Under mobility, the method must be updated, since for the reflected path, the radial velocity and the AoD are estimated simultaneously as both affect the signal across time. The algorithm is as follows (more details can be found in [KKS+22, Algorithm 4])

1. Add the received signal across subcarrier to obtain a vector, whose length is the number of OFDM symbols.

2. Apply elementwise multiplication of this vector and the conjugate of RIS response across time for multiple candidate AoDs. By doing so, if the candidate AoD is equal to the real AoD, the effects of the phase shifts caused by using different RIS phase profiles are removed and only the Doppler effects remain across time.

3. To estimate the radial velocity, apply FFT to all the vectors generated in Step 2.

4. Find the entry with the highest amplitude over all the vectors generated in Step 3. The corresponding AoD and the FFT row will determine the estimate of the AoD and the radial velocity.

5. Refine the estimation by using quasi-Newton algorithm starting from the values in Step 4.

Results and outcomes

Indicative results from [KKS+21] are shown in Figure 4-4. It is observed that the LoS path ToA can be estimated with higher accuracy than the RIS path ToA, since the LoS path is much stronger. For the AoD, both azimuth and elevation angles can be estimated with good accuracy.
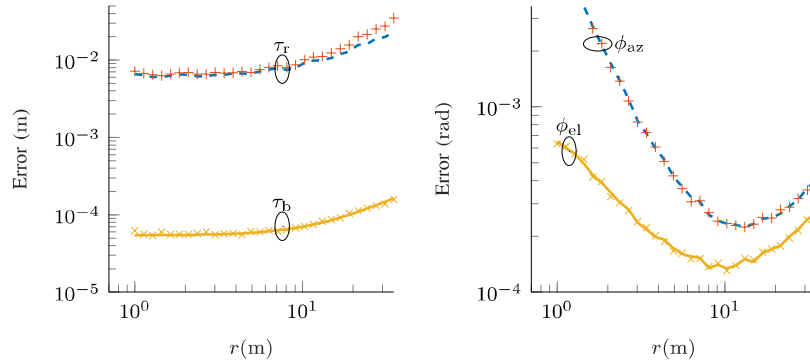
Figure 4-4. Estimation performance as a function of the distance of the UE from the RIS. ToA estimation of the LoS path and RIS path (left). AoD estimation of the RIS path (right). Full lines indicate the CRB, while markers are the estimator performance.

Figure 4-5 and Figure 4-6 show the error bounds and the estimation error for the AoD in azimuth and elevation. The setup includes a BS at [5,5,0] the UE at [-5/√2, 5/√2, -10] and a RIS at the origin. We consider directional and random RIS phase profiles and evaluate the estimation error and the Cramér-Rao bounds (CRB) for the AoD. At low SNRs for the random RIS phase profile, the estimator fails to estimate the AoD, and at high SNRs the error saturates since the error caused by spatial-Wideband (WB) effects becomes dominant.
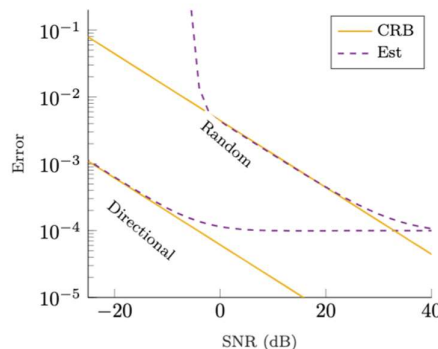
Figure 4-5: Estimation error for AOD azimuth vs the received SNR of the direct path for the user position at [−5/√2, 5/√2, −10]
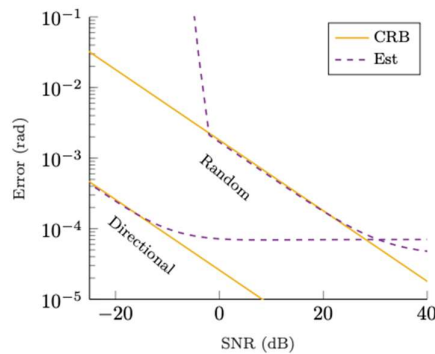
Figure 4-6: Estimation error for AOD elevation vs the received SNR of the direct path for the user position at [−5/√2, 5/√2, −10]

Perspective and relation to other WP5 contributions

ToA estimation is considered, which can be used in structured channel estimation in other WPs. AoD and radial velocity estimation can be used in other WPs for performing structured channel estimation. Also, the model for the wideband effects and Doppler shift can be used for communication purposes.

4.2.2 Contribution #A-2: Far-field ToA and AoD estimation in full-duplex of a signal reflected by a RIS

Motivation and context

This contribution considers a full-duplex UE, which transmits pilot signals and receives the back-propagated signals from controllable RIS and landmarks in the networks, as shown in Figure 4-7. The channel is modelled by the form of the summation of the geometric functions for all paths. The functions consist of the RIS phase, delay, and channel gain for the RIS path, and delay and channel gain for multipath. The RIS phase profile is designed to remove the multipath signals from the received signals. Then, the time delay for the RIS path can be estimated for all OFDM symbols, while the information about AoDs at the RIS (i.e., AoD from RIS to UE) are available to the UE (exchanged as a part of control information) [KSA+22].
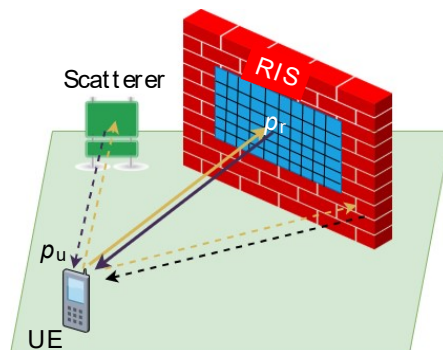
Figure 4-7: System setup with a single-antenna UE and an RIS.

Methodology

It should be noted that sufficient suppression of the transmit signal is assumed so that the backscattered signal is not impacted by transmit signal interference. The RIS phase profiles are designed to distinguish the RIS path signal from the uncontrolled multipath and to form directional beams in different predetermined AoDs. Owing to the codebook design of the RIS phase profile, multipath can be removed, as detailed in [KSA+22, Sec. III-A]. The ToA for the RIS path

and all OFDM symbols is estimated by finding a value maximizing the cost function, formulated by the Inverse Fast Fourier Transform (IFFT) of the received RIS path signal.

Results and outcomes

Performance is equivalent to what is presented in Section 4.2.1.

Perspective and relation to other WP5 contributions

ToA estimation and AoD estimation in a full-duplex setting can be used for monostatic sensing applications. Extension to Doppler processing is straightforward.

4.2.3   Contribution #A-3: Near-field ToA and AoD estimation of a signal reflected by a RIS

Motivation and context

The aim of this contribution is to estimate the ToA and the AoD (in azimuth and elevation) of a downlink signal transmitted by a single-antenna BS, reflected through a RIS and received at a single-antenna UE under geometric near-field conditions, as shown in Figure 4-8. Due to large RIS size and small BS-RIS and RIS-UE distances, both the BS and the UE are assumed to lie in the near-field of the RIS. In addition, it is assumed that the LOS path between the BS and the UE is blocked and no uncontrollable multipath component exists (i.e., the downlink communication from the BS to the UE occurs only through the RIS). Moreover, the BS transmits a narrowband signal, which implies that ToA information cannot be directly extracted from the observations and near-field localisation of UE can only be performed by exploiting the wavefront curvature. Through the Jacobi-Anger expansion-based approximation of the RIS steering vector, AoD and ToA estimation thus becomes possible [OKW+22].
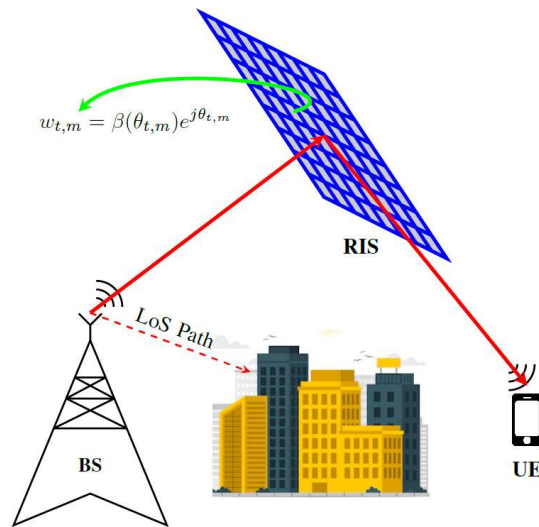
Figure 4-8: RIS-enabled near-field localisation under LOS blockage

Methodology

In the considered setup, the received signal at the UE consists of multiple scalar near-field observations corresponding to multiple transmission instances. The methodology to estimate AoD and ToA from these observations is described as follows:

1. The near-field RIS steering vector is approximated by its far-field counterpart to make it amenable to algebraic manipulations.

2. The Jacobi-Anger expansion of the far-field steering vector is derived using a sufficient number of terms in the approximation as the Bessel function in the expansion decays to zero after a certain approximation order.

3. The resulting approximation of the RIS steering vector can be written as a matrix-vector multiplication, where the matrix and the vector are functions of AoD in azimuth and elevation, respectively.

4. Based on the corresponding observation model derived from this approximation, the AoD in azimuth is estimated via a one-dimensional search.

5. Using the estimated AoD in azimuth, the AoD in elevation can similarly be found via a line search.

6. Finally, using the AoD estimates in azimuth and elevation, the distance (i.e., ToA) between the BS and the UE can be computed via a line search by employing the position-dependent near-field steering vector, where search over distance is carried out by substituting the estimated azimuth and elevation AoDs into the position vector.

The proposed methodology enables reducing the three-dimensional search over the position to three one-dimensional searches, thus significantly reducing the computational complexity of localisation.

Results and outcomes

The results reported in Figure 4-9 show that the UE positioning accuracy can meet the corresponding theoretical bounds already at medium SNR levels (around 5 dB), indicating the effectiveness of the near-field ToA and AoD estimation approach based on the Jacobi-Anger expansion.
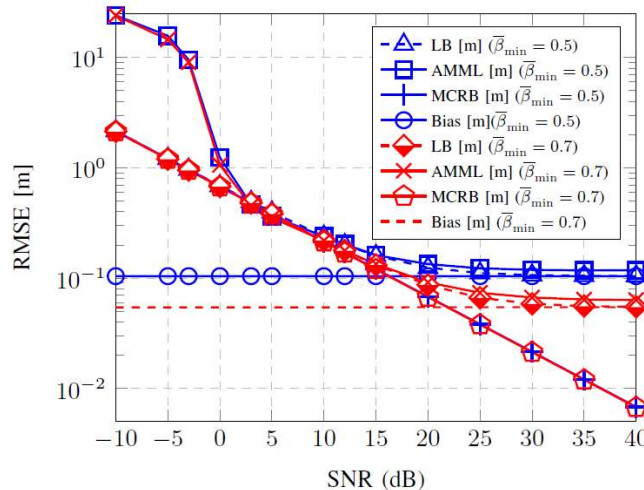
Figure 4-9: Position RMSE of the Jacobi-Anger based method (AMML) along with the corresponding theoretical lower bounds (LB) and the high-SNR asymptotes (bias).

Perspective and relation to other WP5 contributions

The proposed Jacobi-Anger expansion approach could be used in other WP5 contributions studying near-field localisation and sensing scenarios to estimate AoD and ToA.

4.2.4   Contribution #A-4: AOA estimation at a sensing RIS

Motivation and context
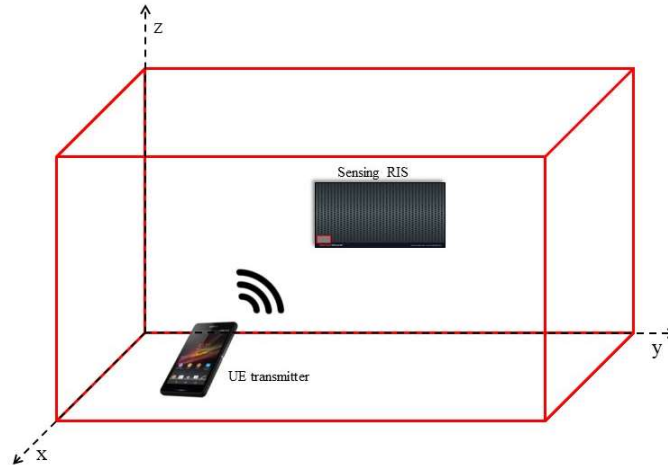
Figure 4-10: AoA estimation at a sensing RIS.

This contribution capitalizes on the recent developments in sensing RISs of [AV20] and [ASA+21], which are equipped with a single Receive (RX) RF chain. This allows the RIS to measure the incoming signals and use the measurements in order to estimate different channel parameters. In [AVW22], an AoA estimation algorithm is designed which utilizes multiple measurements with different phase configurations at a sensing RIS, from the single-antenna UE. A multipath environment with the sensing RIS mounted on the wall of an indoor room as in Figure 4-10 is considered and both far-field and near-field channel models.

Methodology

The AoA estimation at each RIS, presented in more detail in [AVW22], is explained below.
1. The sensing RIS, receives the uplink signal from the UE with a number of different RIS configurations and forms a received signal vector.
2. A compressed sensing approximation of the received signal vector can be modelled as the multiplication of a sensing matrix that contains the RIS please configurations multiplied with a dictionary matrix with the spatial response vectors at the azimuth and elevation AoA pairs and a sparse vector, the sparsity of which equals the number of paths between the UE and the RIS.
3. The AoA for the LoS only channel is being estimated at the RIS, using a subspace Orthogonal Matching Pursuit (OMP) algorithm.
4. The AoA error bound at each RIS is also being computed through the AoA FIM.

Results and outcomes

Figure 4-11 shows the error bound and the estimation RMSE for the elevation AoA at a 64-element sensing RIS, considering multipath and 64 Discrete Fourier Transform (DFT) beams, vs the transmit power. It can be observed that the angle estimation RMSE approaches the

bound as the transmit power values rise. The small gap that appears, is due to the fact that the error bound computation assumes the channel is comprised of LoS only.
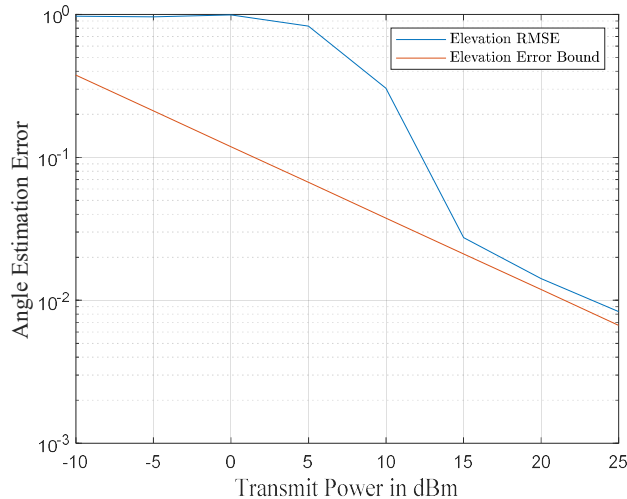
Figure 4-11: Elevation AoA RMSE and elevation error bound vs the transmit power for a sensing RIS at [0,5,7] from a UE at [4,8,2].

Perspective and relation to other WP5 contributions

This AoA estimation technique can also be used for hybrid reflecting and sensing RISs [ASA+21]. AoA estimations from multiple RISs can be combined in order to estimate the UE position, as seen in Contribution #B-5.

5 Estimation of active UE location

5.1 Motivations and challenges

As already mentioned in the previous section, the localisation of connected UEs is generally fed by location-dependent channel parameters or radio metrics, which are preliminarily estimated out of received radio signals from/by these UEs (i.e., T(D)oA, AoA, and AoD, RSSI…). In this second localisation step (but also when performing positioning directly out of the received signals, with no intermediary channel estimation step), the UE(s) position(s) must be determined by means of model-based estimation algorithms, which aim at harnessing statistical relations between the extracted radio metrics and the signal propagation geometry (incl. the location(s) of the UE(s) involved in radio links).

These location estimation algorithms can usually take multiple forms and embodiments, depending on the operating context and constraints (e.g., aiming at addressing a certain trade-off between complexity and accuracy). In the related literature, one can for instance find basic non-probabilistic estimators (e.g., (Weighted) Least Squares between measured radio metrics and estimated metrics based on estimated locations…), probabilistic estimators including both non-Bayesian approaches, such as the Maximum Likelihood (ML) estimator (when the UE location is assumed to be unknown deterministic parameters), and Bayesian approaches (when the UE location is assumed to be random with a certain prior probability distribution), such as the Minimum Mean Squared Error (MMSE) or the Maximum A Posteriori (MAP). The latter encompass dynamic tracking algorithms, such as the (Extended) Kalman Filter or the Particle Filter (PF). Finally, the positioning problem can be solved through statistical inference over graphs with Message-Passing (MP) methods, such as the Belief Propagation (BP) algorithm or one of its multiple variants…

Beyond, in our more specific RIS context, (i) the BS-RIS-UE deployment scenario, (ii) the RIS operating mode (e.g., reflective, receive or hybrid), (iii) the transmission scheme (e.g., multi-carrier or narrow-band, uplink/downlink or both, etc…), (iv) the nature of extracted radio metrics (time-based, power-based, angle-based, etc…) or even (v) the underlying propagation regime considered to model the RIS response (e.g., near field vs. far field)… will not only dictate the choice of certain estimation strategies (or at least, eliminate algorithmic families), but it also discloses new opportunities and challenges, as follows:

- Generally speaking, the presence of RIS(s) over several segments of the radio links imposes to revisit the derivation of theoretical localisation performance bounds (for further benchmark with the proposed estimation algorithms).

- By nature, the localisation algorithms relying on reflective RISs belong to the family of multipath-aided algorithms, which make use of controlled multipath components in addition to -or even as a substitution to- the direct path (if only the latter is present).

- In particular system settings, reflective RISs should provide inherent self-synchronization capabilities among the generated paths (typically, the direct path and a reflected path, or even between two distinct reflected paths), thus relaxing the usual constraints on time-based positioning approaches and/or making at least possible the joint estimation of both UE(s) location(s) and Tx timing uncertainty.

- For RIS-enabled multipath-aided schemes, complex data association problems (typically, between radio observations and modelled location-dependent variables) may need to be solved out, either prior to -or jointly while- applying location estimation. This task may be even more complex as RIS-induced multipath must be distinguished from natural (i.e., uncontrolled) multipath reflections or scattering.

- Depending on the signalling and transmitted waveforms, the location estimation algorithm may necessitate the application (and hence, the knowledge) of particular RIS configurations (in terms of both profiles and/or sequences over time) so as to make the positioning results meaningful or even simply exploitable.

- The possibility to operate with (very) large surfaces (e.g., in reflective, receive or hybrid modes) calls for algorithms that are capable of interpreting the signal wavefront curvature and hence, to benefit from nearfield propagation properties. This could for instance enable direct UE positioning out of received signals without necessitating intermediary angles estimation prior to triangulation (i.e., unlike in usual far field approximations).

- Ideally, the estimated location should also come with an estimation of its uncertainty.

Note that some of the challenges listed above are common to RIS-enabled passive localisation, as seen in section 6.

5.2 Contributions from RISE-6G

An overview of the different contributions is provided in Table 5-1.

Table 5-1 An overview of active UE location estimation contributions

Architecture	Cont. #B-1: Semi-passive Localisation of Multiple RIS Enabled Users	Cont. #B-2: RIS-Enabled SISO Localisation under User Mobility and Spatial-Wideband Effects	Cont. #B-3: RIS-Enabled Self-Localisation: Leveraging Controllable Reflections with Zero Access Points	Cont. #B-4: RIS-aided Near-Field Localisation under Phase-Dependent Amplitude Variations	Cont. #B-5: Localisation via multiple sensing reconfigurable intelligent surfaces, without any BSs	Cont. #B-6: RIS-Enabled Joint Mobile User Location and Velocity Estimation in Near-Field
Nr BS	1	1	0	1	0	1
Nr RIS	Multiple	1	1	1	At least 2	1

Nr UEs	Multiple	1	1	1	1	1
UE Mobility	Stationary	Mobile	Stationary	Stationary	Stationary	mobile
RIS Type	Reflective	Reflective	Reflective	Reflective	Sensing	reflective
Localisation functionality placement	At Rx	At UE	At UE	At UE	At RIS	At UE
Setup						
Uplink/Downlink	DL	DL	UL	DL	UL	DL
Indoor/out-door/UAV	Outdoor	Outdoor	Outdoor	Indoor/outdoor	Indoor/outdoor	Indoor/outdoor
Frequency Band	30 GHz	28 GHz	28 GHz	28 GHz	30 GHz	28 GHz or sub-6 GHz
Narrow-band/wideband	Wideband	Wdeband	Wideband	NB	NB	NB
Near field/far field	Far field	Far field	Far field	NF	Both	NF
LOS/NLOS (BS-RIS-UE)	LOS (Tx-Rx) and NLOS (Tx-RIS-UE)	LOS (BS-UE) and NLOS (BS-RIS-UE)	LOS (UE-RIS-UE)	NLOS	RIS- UE LOS/NLOS	NLOS
Imperfections or other hardware considerations	-	-	-	Phase-depend-ent RIS ampli-tude variations	-	Single antenna BS and UE
Measurement type	ToA and AoD	ToA and AoD	ToA and AoD	ToA and AoD	AoA	direct
RIS configura-tion strategy	Random	Directional	Directional	Random	Random or DFT	Random, direc-tional and ex-tended to optimal
Who collects measurements	Rx	UE	UE	UE	RIS	BS
Synchronisation	Unsynchro-nized	Unsynchro-nized	No	No	No	unsynchronized
Metric optimised	No optimization	No optimization	No optimization	No optimization	No optimization	Wavefront curva-ture

5.2.1   Contribution #B-1: Semi-passive localisation of multiple RIS enabled users

Motivation and context

In this contribution, the aim is to estimate the multiple UE locations in a semi-passive localisation scenario, where a single Tx and multiple Rxs are allocated. Each of UE is equipped with an RIS, and the Tx and Rxs are equipped with a single antenna. The Rxs receive the propagated signals consisting of LOS (Tx-Rx) and NLOS (Tx-UE-Rx and Tx-scatter-Rx). The scenario was depicted in Figure 4-2. This localisation problem is challenging due to the following reasons:

1. The data association between the measurements and UEs is unknown.
2. The time between Tx and RXs is not synchronized.

Methodology

The ToA measurements (that are estimated in section 4.2.1) are used in estimating the UE locations. To handle the clock bias, referring to the time difference between Tx and Rxs, the TDoA measurements are considered, and the LOS path is used as a reference to eliminate the clock bias. Then, at each Rx, the TDoA measurements for all UEs are determined, and the UE localisation problem is formulated as a Least Squares (LS) problem, which is solved via the gradient descent algorithm.

Results and outcomes

Figure 5-1 shows the CDF of the PEB and the estimation error for 100 RIS configurations. It is confirmed that the proposed UE estimator can attain the PEB as long as the PEB is less than about 8 m. Figure 5-2 shows the PEB and the UE estimation error in the presence of additional scatterers. It is then shown that the estimator can perform well in the scenario, where there are a large number of scatterers.
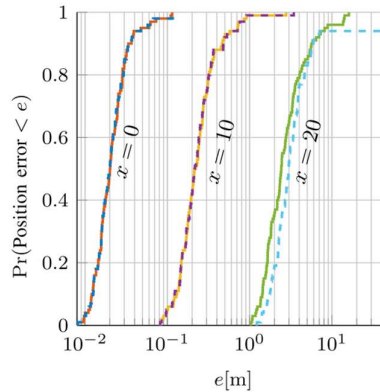
Figure 5-1: CDF of PEB (solid lines) and estimation error for 100 random RIS configurations at [x,0,-3].
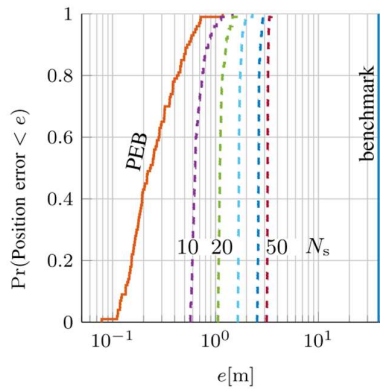
Figure 5-2: Average PEB (solid line) and the estimation error (dashed line) for 100 random RIS configurations at [10,0,-3] meters in the presence of 10, 20, 30, 40, and 50 scatterers.

Perspective and relation to other WP5 contributions

The UE location estimator can be used as the part of UE localisation for the detection of passive objects and SLAM (See section 6).

5.2.2   Contribution #B-2: RIS-Enabled SISO Localisation under User Mobility and Spatial-Wideband Effects

Motivation and context

The aim of this contribution is to estimate the UE location based on the received signal from the BS and reflected signal from an RIS by addressing the UE mobility and spatial-wideband effects. The BS and UE are equipped with a single antenna, and the RIS is a uniform planar array. The scenario was depicted in Figure 4-1. For the first time in the literature, the problem of single-snapshot RIS-aided SISO localisation under UE mobility and spatial-WB effects is addressed.

Methodology

The ToAs and AoD measurements (that are estimated in section 4.2.1) are used in estimating the UE location. First, the direction of the UE based on the AoD. Second, the distance between the UE and the RIS is estimated by formulating a least squares problem, and solved via the gradient descent method. Then, the UE location is determined by the estimated direction and distance from the RIS.

Results and outcomes

Figure 5-3 shows the estimation error and the CRB for UE position. It is confirmed that the estimator attains the PEB, and spatial-wideband degrades the localisation accuracy. The effect of the directional beamforming is more pronounced than the random phase, due to higher SNRs in the directional case, which makes the distortion more pronounced. Figure 5-4 shows the CDFs of the estimation error and the CRB of random and directional RIS phase profiles. The high-mobility of user slightly degrades the accuracy of the velocity estimation. However, it does not affect the accuracy of the UE position estimation.
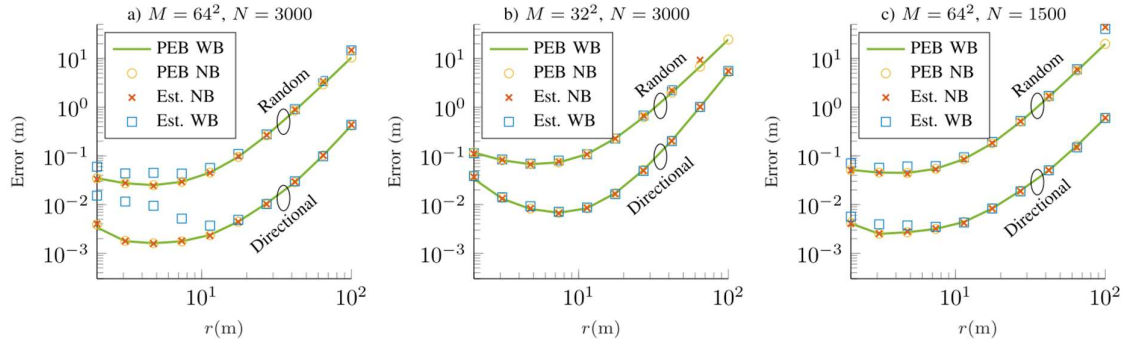
Figure 5-3: Estimation error and the CRB for UE position along the path [-r/√2, -r/√2,-10], where r varies between 2 m to 100 m, and directional and random RIS phase profiles.
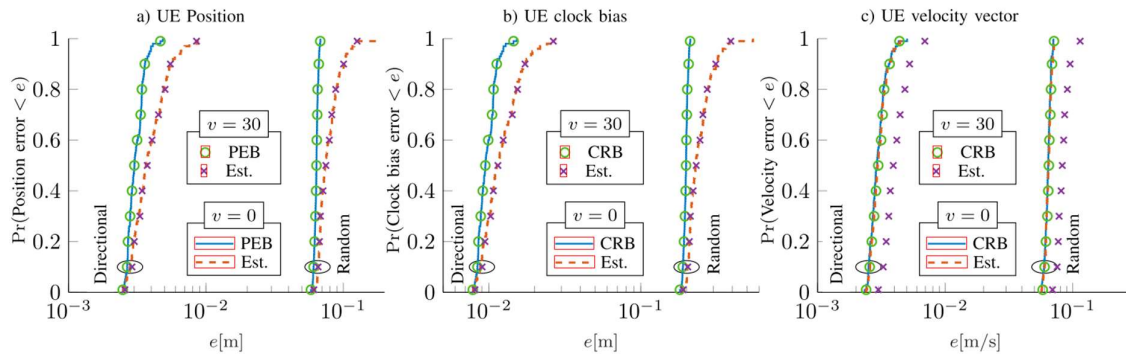
Figure 5-4: CDF of estimation error and CRB bounds of directional and random RIS phase profiles for a) UE position, b) UE clock bias, and c) UE velocity. The UE has the position [-10,10,-10] with the velocity $[-v, v, 0]$, where v is between 0 and 30 m/s.

Perspective and relation to other WP5 contributions

The UE state (position, clock bias, velocity) estimator can be used as the part of UE localisation for the detection of passive objects and SLAM (See section 6).

5.2.3 Contribution #B-3: RIS-Enabled Self-Localisation: Leveraging Controllable Reflections with Zero Access Points

Motivation and context

This work aims to open a RIS-enabled self-localisation area that is enabling the UE to estimate its own position in far-field scenarios of zero-base stations. The UE, equipped with the SISO antenna, transmits the pilot signals and receives the back-propagated signals from controllable RIS and landmarks in the networks. The channel is modelled as the summation of the geometric functions for all paths. The functions consist of the RIS phase, delay, and channel gain for the

RIS path, and delay and channel gain for multipath. The RIS phase profile is designed to remove the multipath signals from the received signals. Then, the time delay for the RIS path can be estimated for all OFDM symbols, while the information about AoDs at the RIS (i.e., AoD from RIS to UE) are available to the UE (exchanged as a part of control information). Consequently, the UE position can be estimated from the time delay and AoDs.

Methodology

We estimate the UE position by using the time delay and AoD of the RIS phase profile (of the RIS path) for all OFDM symbols without the data association between channel parameters and sources. First, we design the RIS phase profile to distinguish the RIS path signal from the back-propagated signals. Owing to the codebook design of the RIS phase profile, multipath can be removed, as detailed in [KSA+22, Sec. III-A]. Second, the time delay for the RIS path and all OFDM symbols is estimated by solving an optimization problem, where the cost function is formulated as the inverse fast Fourier transform of the received RIS path signal. Then, the UE can utilize the estimated time delay and pre-defined AoD of the RIS phase profile to estimate its own position. This is done by first computing a coarse estimate of the relative UE position, and then refining it via maximum likelihood estimation based on Newton algorithm.

Results and outcomes

Figure 5-5 shows the positioning error of the proposed method. The beam towards random points inside the uncertainty area of the UE location is generated for the directional codebook. With the higher distance d, the positioning error increases by about sub-meter, and UE localisation is still possible. However, the performance cannot achieve the PEB due to the low SNR. Figure 5-6 shows the CDFs for the PEB (solid lines) and estimation errors (dashed lines) for the UE position at d = 11 m. The performance of UE position estimates approximately follows the PEB. Figure 5-7 shows the effects of RIS size on the PEB. The PEB of the directional phase profile significantly decreases with the number of RIS elements increasing, compared to the random codebook, due to the high SNR at directional beamforming.
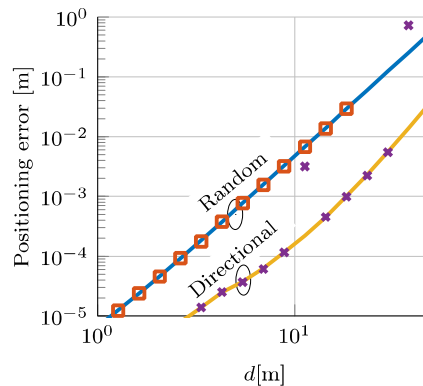
Figure 5-5: Estimation error (markers) and PEBs (solid lines) for a UE position at $[d, d, d]/\sqrt{3}\ [m]$.
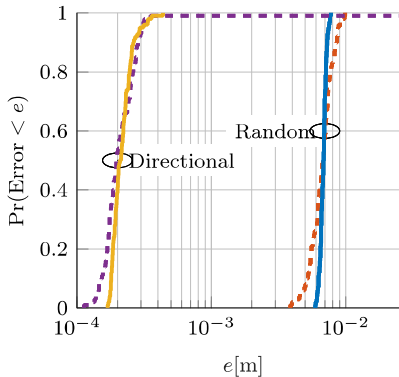
Figure 5-6: CDF of the estimation error (dashed lines) and PEB (solid lines) for d = 11 m and 100 realizations of PIS phase profiles.
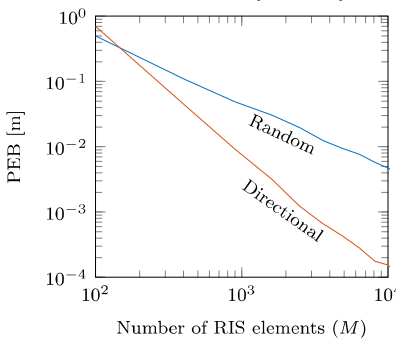
Figure 5-7: PEB at a UE position $[10, 10, 10]/\sqrt{3}$ for different RIS sizes and for directional and random codebooks.

Perspective and relation to other WP5 contributions

The time delay estimation in RIS-enabled self-localisation in zero BSs can be used in other WPs for performing the channel estimation routine for communication purposes.

5.2.4   Contribution #B-4: RIS-aided Near-Field Localisation under Phase-Dependent Amplitude Variations

Motivation and context

In most studies on RIS-aided localisation, RIS elements are assumed to have unit-amplitude responses. However, realistic hardware modelling based on equivalent circuit models of individual reflecting elements shows that RIS amplitudes change as a function of the applied phase shifts [AZW+20], as illustrated in Figure 5-8. This contribution aims to investigate theoretical bounds and algorithms for RIS-aided near-field localisation of a single-antenna UE using downlink signals transmitted by a single-antenna BS under the practical model of phase-dependent RIS amplitude variations for the scenario depicted in Figure 4-8. In particular, localisation performance degradations due to such variations will be analysed by resorting to the miss-specified CRB (MCRB) analysis, and joint localisation and online RIS calibration algorithms will be introduced to be able to find UE location while estimating the circuit-specific parameters of the RIS amplitude model.
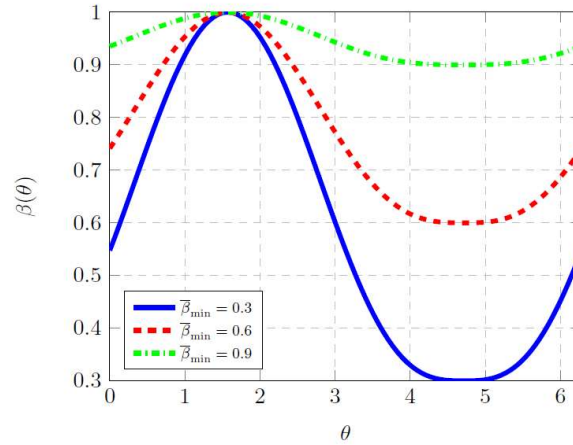
Figure 5-8: RIS amplitude variations as a function of the applied phase shift for three different values of the RIS circuit parameter β_{min} [AZW+20]

Methodology

The methodology consists of two parts: MCRB computation to investigate performance penalties and algorithm development for joint localisation and RIS parameter estimation (i.e., RIS calibration).

The steps to compute the MCRB are as follows:

1. Pseudo-true parameter is estimated by solving the problem of minimizing the Kullback-Leibler (KL) divergence between the true probability density function (pdf) (with amplitude variations) and the assumed pdf (with unit-amplitude RIS elements).
2. MCRB is derived as a function of the pseudo-true parameter using the true and assumed signal models.

The algorithm for joint localisation and online RIS calibration is described as follows:

1. Initialization of UE location via Jacobi-Anger expansion based ToA and AoD estimation algorithm in Contribution #A-3.
2. Online RIS calibration by iterative update of channel gain and individual parameters of the RIS amplitude model.
3. Refinement of UE location and channel gain using the calibrated RIS model.

Results and outcomes

For simulation analysis, three scenarios are considered:

- Scenario-I: The UE is unaware of the RIS amplitude variations and assumes unit-amplitude RIS responses, where the performance bounds are obtained via the MCRB analysis.

- Scenario-II: The UE is aware of the RIS amplitude variations model but does not have the knowledge of the model parameters, where the performance bounds are obtained via the standard CRB analysis.

- Scenario-III: The UE has the knowledge of the RIS amplitude model parameters.

Figure 5-9 shows the results of the theoretical performance analysis for these scenarios, which indicates an order-of-magnitude degradation in localisation performance at high SNRs. Hence, being unaware of the RIS amplitude variations can be an important limiting factor for high-accuracy localisation. Figure 5-10 reports the RMSEs obtained by the proposed localisation and RIS calibration algorithm and the corresponding bounds, where the approximate mismatched

maximum likelihood (AMML) and the approximate maximum likelihood (AML) variants of the algorithm are employed under Scenario-I (mismatched case) and Scenario-II/III (matched case), respectively. As seen from the figure, the proposed algorithm under Scenario-II can successfully recover the performance loss due to model mismatch, reaching the accuracy achievable under Scenario-III, and achieve the CRBs with a calibrated RIS model.
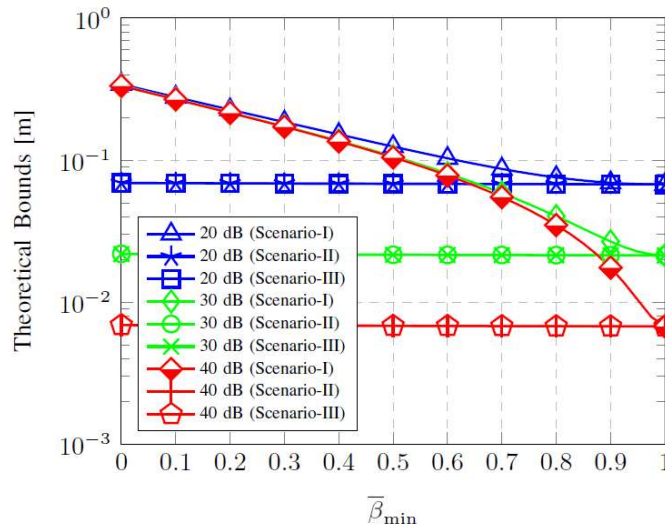
Figure 5-9: Theoretical bounds for three different scenarios under phase-dependent amplitude variations, plotted with respect to the β_{min} parameter of the RIS amplitude model.
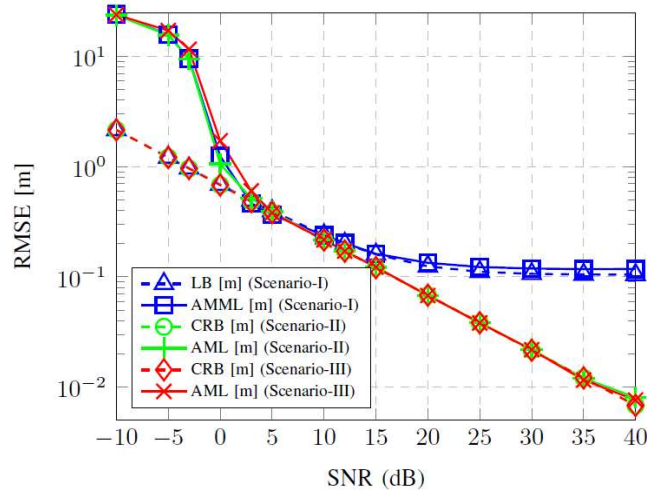
Figure 5-10: RMSE performance of the localisation algorithm under Scenario-I (AMML) and Scenario-II and III (AML).

Perspective and relation to other WP5 contributions

This contribution relies on the near-field ToA and AoD estimation method proposed in Contribution #A-3. The proposed online RIS calibration method can be employed in other WPs dealing with RIS hardware imperfections.

5.2.5 Contribution #B-5: Localisation via multiple sensing reconfigurable intelligent surfaces, without any BSs

Motivation and context
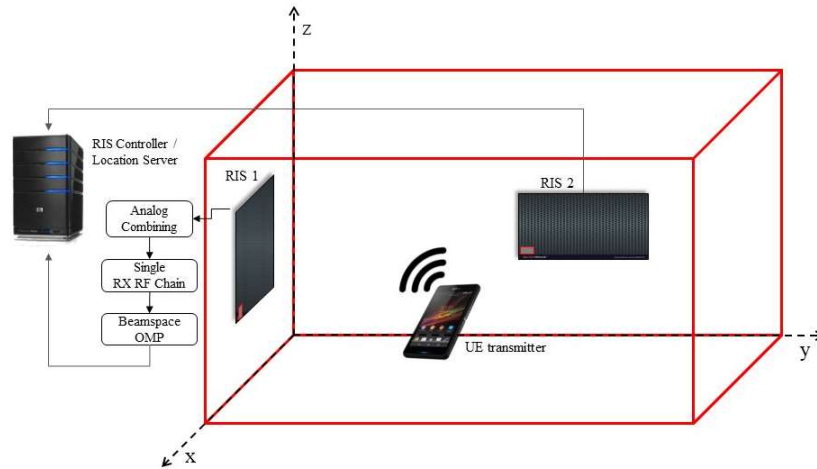
Figure 5-11: UE localization via multiple sensing RISs system setup.

This contribution, found in more details in [AVW22], aims to localise a single-antenna UE with multiple sensing RISs, each equipped with a single Receive (RX) RF chain [AV20], [ASA+21], without the presence of a BS. In a multipath indoor environment with sensing RISs on the walls, as depicted in Figure 5-11, considering free-space pathloss, AoA estimations from each sensing RIS are fused at a central controller in order to estimate the 3D UE position.

Methodology

1. Each sensing RIS, receives the uplink signal from the UE with a number of different RIS configurations and forms a received signal vector.
2. The AoA for the LoS only channel is being estimated at each RIS, using a subspace Orthogonal Matching Pursuit (OMP) algorithm, along with the AoA error bound through the AoA FIM.
3. Using a least squares intersection of lines technique that takes the AoA estimations from each RIS as inputs, a first UE position estimation is computed, which is then input to a Maximum Likelihood algorithm that localizes the UE at the central controller.
4. The PEB is also computed through combining the individual FIM matrices of each RIS.

Results and outcomes

In Figure 5-12, the impact of the RISs' placement on the PEB and the overall coverage is being studied by presenting the empirical CDF of the PEB for various UE positions and RIS placements. Placing the RIS on different walls is better for overall coverage, while for better localization accuracy near a single wall, placing RISs on the same wall is preferred. The case of placing RISs on the same heights appears better for localization performance, while the case of different heights leads to better overall coverage. In Figure 5-13, the impact of the number of RISs and the type of channel model on the localisation performance is being studied under both Far Field (FF) and Near Field (NF) channels, along the PEB for the FF case. It can be observed that the

proposed ML-based localisation technique approaches the PEB as the transmit power rises. Reasonably, the PEB gets lower by increasing either the number of RISs or the transmit power. The RMSE curve saturation for the NF channel model case compared to the PEB is due to channel model mismatch and for the FF channel model is due to the multipath channel model.
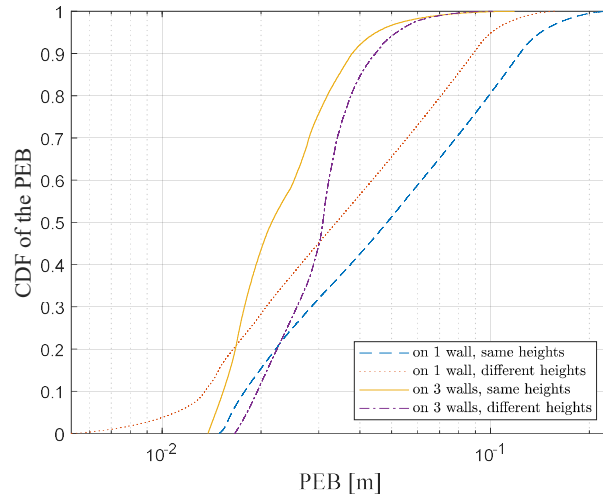
Figure 5-12: The empirical CDF of the PEB for various UE positions with the third dimension of its position vector fixed at 5m, transmit power of 10 dBm and three 64-element sensing RISs at different placements on the room's walls were considered.
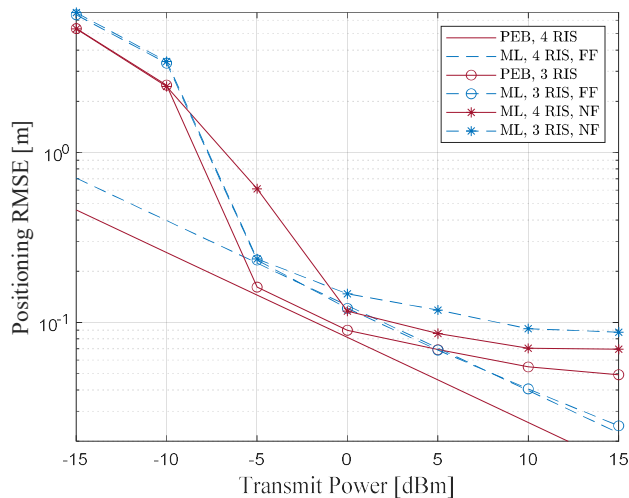
Figure 5-13: The RMSE of the positioning error with the ML-based positioning technique in meters versus the source transmit power in dBm considering 3 and 4 RISs, each with 64 unit elements, placed at [0,5,7], [5,0,1], [10,6,8], and [4,10,6], along with the PEB. The UE was positioned at [4,8,2] and 64 quantized DFT phase profiles were used for each RIS. Both the FF and NF channel models were considered.

Perspective and relation to other WP5 contributions

This contribution is a localisation method based on the sensing RIS AoA estimation technique of Contribution #A-4. In this localisation method, instead of sensing RISs, hybrid reflecting and sensing RISs [ASA+21] can be used.

5.2.6 Contribution #B-6: RIS-Enabled Joint Mobile User Location and Velocity Estimation in Near-Field

Motivation and context

Single RIS reflections have already shown promising potential for SISO positioning out of DL transmissions in static nearfield conditions, enabling in particular localisation continuity in NLoS conditions based on random RIS configurations (with moderate accuracy though) [RDK+21] and beyond, through RIS phase profile optimization based on position error bounds minimization [RDK+22a]. However, the possibilities offered by nearfield propagation still look largely underexploited in dynamic NLoS scenarios.

One motivation to this work is thus to show how large reflective RISs can enable the joint (direct) estimation of both mobile user's 3D position and velocity (i.e., somehow leveraging the small-scale Doppler effects observed at the various RIS elements) [KKS+22], while still relying on sequences of DL transmissions in a simple SISO configuration. For this purpose, both theoretical bounds and practical estimators need to be investigated and evaluated.

Methodology

We have first modelled explicitly the received signal as a function of UE's 3D position and velocity variables, while using a generic reflective RIS near field response formalism. Then, we have specified relevant channel and positional parameters with respect to the stated estimation problem and accordingly, we have calculated the Fisher Information Matrix (FIM) to derive the corresponding CRB characterizing position [RDK+21] and velocity [CJG+22] estimation errors. Those bounds have been evaluated as a function of key system parameters.

Results and outcomes

Theoretical Cramer-Rao lower bounds on the estimated position of a dynamic UE are derived with respect to the distance between the latter and the RIS, the curves are plotted in Figure 5-14 with two different velocities and two different RIS profile designs, i.e., random and directional (with uncertainty sphere of radius = 0.5 m). The same simulation is run to derive the velocity error bound (VEB) at different UE-RIS distance while considering a constant velocity for the measurement window and the curves obtained are displayed in Figure 5-15. The results first show how the positioning performance, as well as velocity estimation, degrades as the UE gets farther from the RIS. Moreover, in both figures, the directional codebook design shows enhanced performance over the randomised one, even with the same number of pilot transmissions, due to higher SNR. On the other hand, the velocity of the UE seems not to have any

effect on either of the bounds in either of the codebook designs. Similar effects have been noticed when running a real estimation algorithm [KKS+22].
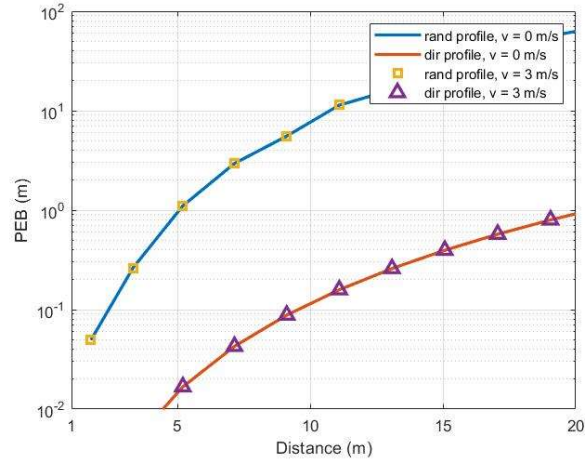
Figure 5-14: Theoretical position error bounds (PEB) vs. distance for a dynamic user with different velocities.
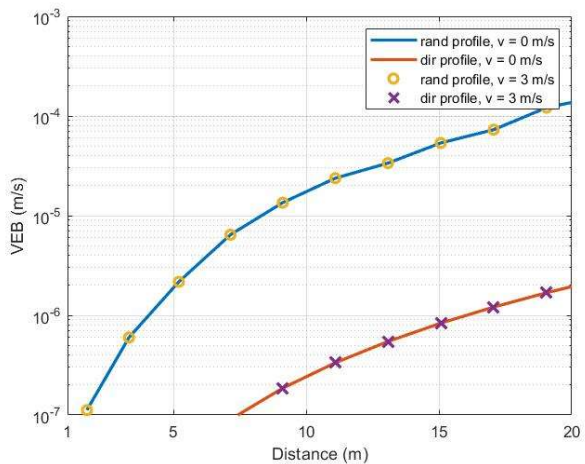
Figure 5-15: Theoretical velocity error bounds (VEB) vs. distance for a dynamic user with different velocities.

Perspective and relation to other WP5 contributions

After deriving the error bounds on both position and velocity, and given a known arbitrary RIS phase profile configuration, a 2-step algorithmic approach, relying on a preliminary coarse estimation step and an iterative refinement step, is currently being implemented. Then, the performance of the proposed algorithm will be evaluated by means of simulations and confronted with theoretical bounds, while considering random and directional RIS phase profiles from [RDK+22a].

Finally, considering a complete dynamic scenario, the previous 3D position/velocity estimation algorithm will be coupled with both a Bayesian tracking filter and a dynamic RIS control mechanism. First, for a given time epoch (i.e., over a sequence of DL transmissions), 3D position/velocity estimates (as produced by the point estimator above) will be further injected as input observations into the tracking filter, whereas the output of the latter (i.e., typically the predicted

3D position/velocity, along with their associated prediction covariance) can be used to further optimize the RIS phase profile for next direct 3D position/velocity estimation steps.

6 Detection of passive (uncontrolled) objects and SLAM

6.1 Motivations and challenges

As observed and explained in the previous sections, the radio environment produces multipath propagation that complicates the location task by interfering with the direct path that carries the information for the true direction and distance of the transmitter. If not dealt with, the extra multipath components will reduce location precision. However, if the multipath components can be resolved, they provide information about the environment and a basis for predicting expected multipath behaviour – as well as possible deviations from the latter.

Here, the role of the RIS can be twofold

- **A reflective RIS** provides an additional, controllable signal path through the environment. As opposed to the passive objects, it can be controlled to support the separation of the RIS path from the others, thereby enabling more accurate (simultaneous) location and mapping (SLAM).

- **A receiving RIS** acts as a large dimensional array or a phased array and observes the incoming signal for further processing. The observations are used for mapping the environment, thereby supporting the detection of changes in the environment.

6.2 Contributions from RISE-6G

An overview of the different contributions is provided in Table 6-1.

Table 6-1 An overview of SLAM and passive object detection contributions

Architecture	Cont. #C-1: RIS-Enabled Self-localisation and SLAM with Zero Access Points	Cont. #C-2: Assessing Wireless Sensing Potential With Large Intelligent Surfaces	Cont. #C-3: Radio Sensing with Large Intelligent Surface for 6G	Cont. #C-4: AI-based intrusion detection using Intelligent Surfaces at mmWave
Nr BS	0	0	0	1 or more
Nr RIS	1	1	1	Multiple
Nr UEs	1	Single	Multiple	Multiple
UE Mobility	Moving	Moving	Moving	Fixed
RIS Type	Reflective	Receiving	Receiving	Reflective
Localisation functionality placement	At UE	At RIS	at RIS	At BS
Setup				
Uplink/Downlink	UL	UL	UL	UL/DL
Indoor/outdoor/UAV	Outdoor	Indoor	Indoor	Indoor
Frequency Band	30 GHz	Sub-6 GHz	Sub-6 GHz	60-GHz
Narrowband/wideband	Wideband	narrowband	narrowband	narrowband
Near field/far field	Far field	Near-field	Near-field	Far-field
LOS/NLOS (BS-RIS-UE)	LOS (UE-RIS-UE) and NLOS (UE-landmark-UE)	LOS and NLOS	LOS	LOS and NLOS
Imperfections or other hardware considerations	-	-	-	Imperfect beam patterns
Measurement type	ToA and AoD	RSS at RIS	Complex signal	RSS at BS and UEs
RIS configuration strategy	Arbitrary	Arbitrary	Arbitrary	Beam sweep
Who collects measurements	UE	RIS	RIS	BS and UEs

6.2.1 Contribution #C-1: RIS-enabled self-localisation and SLAM with zero access points

Motivation and context

The motivation for this work is to show that passive RISs can enable SLAM at the UE (Rx) without BS (Tx). The UE and RIS are equipped with uniform planar array antennas, and UE transmits the signals and receives the back-propagated signals from the RIS, scatterers, and surfaces. This SLAM problem is challenging due to the unknown data association between measurements and landmarks (RIS, scatterers, and surfaces). The scenario is depicted in Figure 6-1.
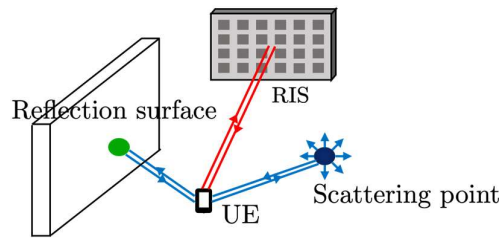
Figure 6-1: System setup with a UE, RIS, reflection surfaces, and scatterers

Methodology

The LoS path can be available due to the codebook design of the RIS phase profile, developed in [KKS+22, KSA+22]. For SLAM, the channel parameters for all paths are used, and standard parametric channel estimation routines can be applied, such as ML, SAGE, or ESPRIT. Even when the passive (uncontrolled) landmarks are not distinguishable, this SLAM problem can be handled by the marginalized Poisson multi-Bernoulli filter [KGS+22], one of random-finite set-based SLAM filters.

Results and outcomes

Figure 6-2 and Figure 6-3 show the RMSE of vehicle location estimates and Generalized Optimal Sub-pattern Assignment (GOSPAs) of virtual anchor (VA) and scattering point (SP), for random and directional RIS phase profile. It is clearly seen that the directional RIS phase has a significant gain in SLAM.
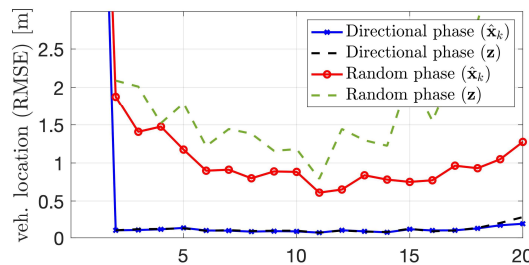
Figure 6-2: RMSE of vehicle location estimates for random and directional RIS phase profile.
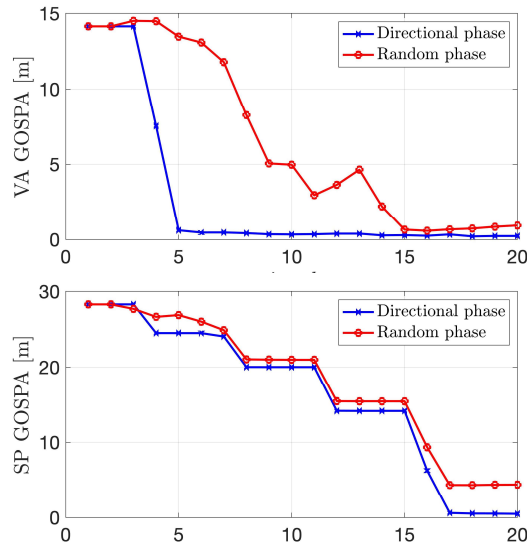
Figure 6-3: GOSPAs of VA and SP for random and directional RIS phase profile.

Perspective and relation to other WP5 contributions

This work, estimating the landmarks and UE location, can be used in other WPs for spatial information-based channel estimation and communication purposes (i.e., context-aware communications).

6.2.2 Contribution #C-2: Assessing wireless sensing potential with large intelligent surfaces

Motivation and context

This work aims to leverage the wireless sensing potential of beyond massive MIMO systems. RISs arise as a powerful solution for wireless communications, however, due to their characteristics they can potentially be used to perform accurate sensing. Then, different parameter designs of these surfaces are evaluated to leverage the impact on the sensing performance. In this work, the evaluation is conducted in an industry 4.0 scenario, to show the high application potential of RIS with receiving capabilities (also called Large Intelligent Surface (LIS)) for sensing tasks. We leverage the sensing potential by solving a trajectory deviation detection of industrial robots by describing the wireless environment as an image. The robots transmit an arbitrary sensing signal, that will be used at the RIS to describe the environment. To perform simulations in the most reliable way, this work resorts on ray tracing. The channel is modelled as the addition of the complex electric fields for every ray path at the antenna elements by assuming isotropic antennas.

Methodology

We perform the trajectory deviation detection based on the received signal power at the RIS. This received signal power is mapped into an RGB image that captures the information of the environment thanks to the RIS characteristics. To solve the problem, we perform a data-driven approach. First, we sample the received signal at the RIS with a period T along the correct trajectory of the industrial robot. Next, we train an unsupervised learning algorithm called Local-Outlier-Factor (LOF) that will learn the clusterized distribution of the received signal along the correct path. As an extra step, we develop a Denoising Autoencoder (DAE) that learns to map the image quality and therefore the sensing performance. Second, we compare these results against a statistical hypothesis test based on the Generalized Likelihood Ratio (GLRT) that is

used as a benchmark. The latter solves the problem by exploiting the large number of antennas on the RIS in the same way as in massive MIMO systems. However, our novel technique follows a completely new approach which relies on the received signal across the surface as a radio image of the environment. What is more, the presented approach is independent of the data distribution and no assumptions are needed for its implementation, on the contrary to the GLRT where we need to assume the noise is Gaussian distributed with known noise variance for the sake of simplicity in the analytical derivations. In reality, these assumptions may not hold.

Results and outcomes

Figure 6-4 shows the impact of inter-antenna spacing on the sensing performance for a deviation in the trajectory of 50/10 cm, leading to the conclusion that performance is enhanced the lower the inter-antenna spacing. For processing, the signal is sampled S times and averaged (Avg) in order to reduce the noise variance contribution and enhance the radio map quality. Figure 6-5 shows the comparison of the benchmark solution against our radio image proposed system. We see the improvement due to the S-average strategy as well as the DAE to enhance the image resolution. We can see our final method (green line) exhibits a good performance even in quite lower SNR conditions, without the need of any assumptions in the received signal and noise distributions. Figure 6-6 shows the performance comparison in all the scenarios presented. We can see that our method works better the closer the deviations of the routes are, thanks to the usage of DAE. This is something that is contrary to standard wireless sensing systems, leading to an advantage in proximity accuracy.
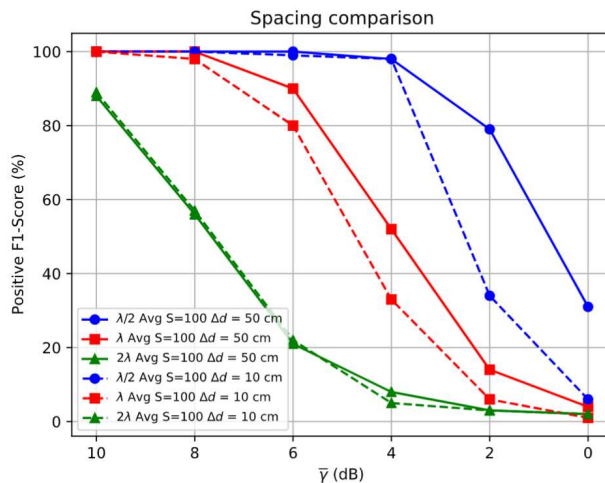
Figure 6-4: PF1 score for radio image sensing with fixed RIS aperture of 5.44 x 5.44 m, correct route parallel to the RIS, anomalous points placed at Δd = 10 and Δd = 50 cm, S = 100 samples, and different number of antennas and spacings.
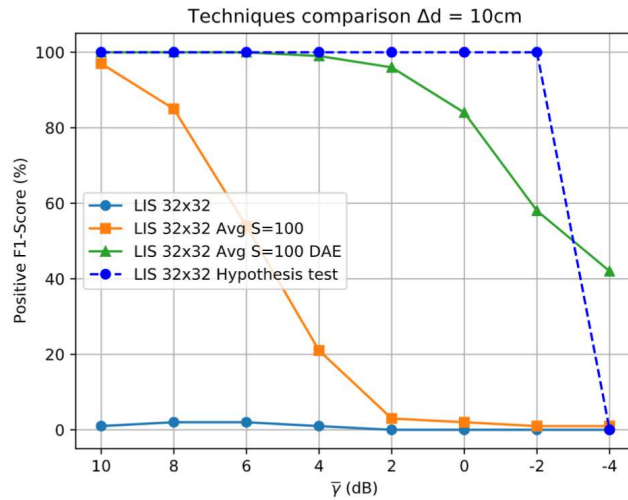
Figure 6-5: Comparison between radio image sensing and the statistical solution for M = 32 x 32 antennas, correct route parallel to the RIS, spacing of λ/2 and different processing techniques.
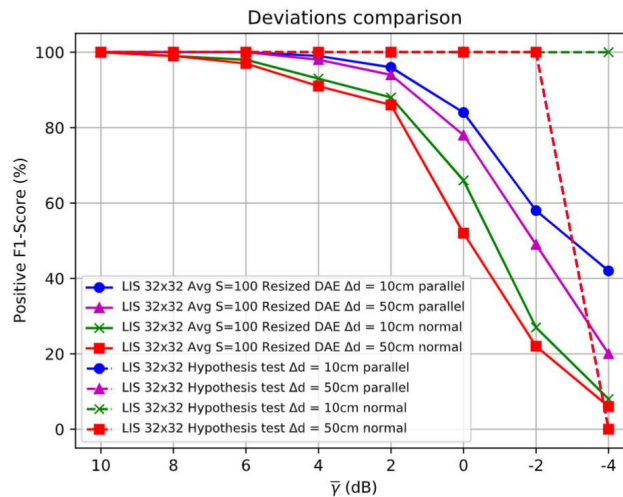
Figure 6-6: Comparison between radio image sensing and the statistical solution for M = 32 x 32 antennas, different correct routes and spacing of λ/2.

Perspective and relation to other WP5 contributions

The RF snapshots of the environment which are a side product could be used for further tasks related to the location of scatterers and in the context of contributions in Section 7 below.

6.2.3 Contribution #C-3: Radio sensing with large intelligent surface for 6G

Motivation and context

Motivated by their future integration in communication systems, in this work, we are focusing on the sensing capabilities of RIS and investigate their potential to detect passive users. Such functionality can be important in human intrusion detection. It also allows to optimize beamforming towards the passive devices already during their initial access phase. We rely on the arbitrary wireless signals occurring in the environment and we process them directly from the RIS viewpoint to obtain a radio map, which describes the physical presence of passive devices. We make use of machine learning, image processing and computer vision to extract meaningful

information from these radio maps. Finally, we evaluate the proposed method for both active and passive user detection in an indoor setting.

Methodology

We assume there are random active devices which are sending communication signals in the environment. Due to the large physical aperture and the proximity between the transmitters and the RIS, spherical wave propagation conditions need to be considered. We then design a spherical-wave match filter that we apply directly to the received complex signal. In this way, we create a radio map in which the active and passive targets are captured due to acting as real and virtual sources, respectively. For the active detection, a maximum filtering procedure is applied along the radio map. For the passive target detection, we process the radio map using k-means clustering to enhance obtained features in the map. We next apply some template matching to remove the active transmitters and apply image processing and component labelling to identify the passive targets.

Results and outcomes

Figure 6-7 shows an exemplary localisation of 10 passive humans in the room. Figure 6-8 shows the average passive (human) detection for different amount of active random devices in the area. The results show the method increases in amount of passive detected humans the higher the number of active transmitters, with a minimum detection of 80% of the people in the scenario. Also, the average positioning error is around 28 cm.
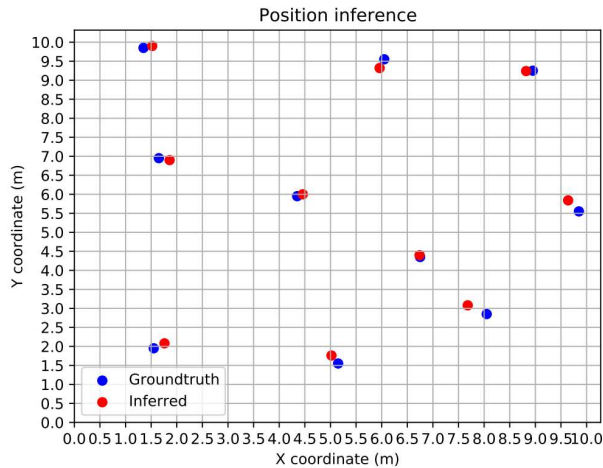
Figure 6-7: Exemplary human detection with fixed RIS aperture of M = 259 x 259, in a γ = 0 dB condition, with S = 100 averaging strategy, Ua = 20 active users and Up = 10 passive users in the scenario.

Figure 6-8: Average human detection percentage (%) and positioning errors (cm) with fixed RIS aperture of M = 259 x 259, in a γ = 0 dB condition, with S = 100 averaging strategy and Up = 10 passive users in the scenario for different numbers of active devices Ua.

Perspective and relation to other WP5 contributions

The radio maps which are a side product could be used for further tasks related to the environmental description and location of scatterers and in the context of contributions in Section 7 below. The active and passive device detection is crucial for the electromagnetic field (EMF) avoidance and management techniques investigated in WP6.

6.2.4 Contribution #C-4: AI-based intrusion detection using intelligent surfaces at mmWave

Motivation and context

The impressive performance of mmWave communications comes at the price of harsher propagation conditions than the ones experienced in the sub-6GHz counterpart, with particularly high attenuation, low diffraction, and high blockage vulnerability, including human bodies, making the communication very sensible to the propagation environment. As a result, mmWave devices require a larger number of antenna elements to provide high spatial processing gains and steering capabilities that compensate for experienced pathloss and overcome transmission blockages and, at the same time, provide spatial diversity to the communication channel opening the possibility of directional channel sounding [DSF+20].

When reconfigurable intelligent surfaces (RIS) are in place, directional channel sounding becomes particularly advantageous (especially in indoor environments) due to the high number of reflections and the absence of atmospheric phenomena (that may unpredictably alter the channel). In particular, triggering properly RIS configurations can be exploited to passively monitor propagation condition changes and infer their cause by checking the feedback coming from the active device.

Methodology

We build on top of the idea of turning the mmWave propagation drawbacks into a useful source of information, opening the possibility to develop novel applications such as environment monitoring, blockage detection, user detection and, in general, localisation.
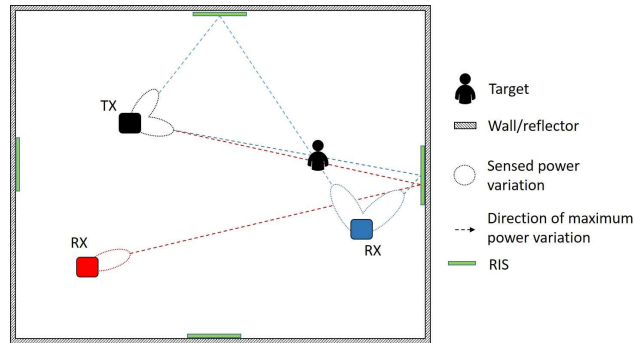
Figure 6-9: Example of passive localisation

Specifically, the indoor localisation framework does not require an active connection with the target, i.e., it performs localisation in a *passive* manner. We therefore exploit RIS beamforming capabilities to directionally sense the propagation environment, detect and track environmental changes to perform people localisation in the area of interest, as depicted in Figure 6-9. In addition, such a solution does not require a change in the existing network deployment but, it can be realized by means of RIS properly deployed in the scenario.

The localisation and tracking framework leverages on the knowledge of *i)* the shape of the available RIS beampatterns, *ii)* the deployment of RIS devices, and *iii)* the position of transmitters in the propagation environment. However, practical scenarios might lack of such accurate description. For example, private customers may not be willing to share information on the deployment of devices for privacy related reasons. To solve such an issue, we leverage an AI-based solution that can automatically approximate the function that links the target position to the RIS beamforming beampatterns by exploiting a self-learning approach that adapts the localisation process to the specific propagation environment and deployed RIS devices' configurations without requiring detailed prior information on the beam patterns, on the position of the transmitters, and on the RIS deployment setup.

Results and outcomes

We numerically assess the performance evaluation of the proposed RIS-based passive localisation framework. We emulate the indoor propagation scenario by means of an ad-hoc MATLAB simulator. In particular, we consider a 10x10m^2 indoor environment surrounded by reflecting walls with 4 RIS devices deployed, working at 60GHz. The codebook of each RIS device comprises 34 beampatterns pointing at equally spaced directions that can be automatically configured.

The beam patterns, the pathloss and the reflection coefficient are modelled as per [FSD+17]. Reflections are taken into account up to the 3rd order reflection, while the temporal distribution of incoming rays is modelled according to [WWS+17] with a number of post-cursors rays set to 3. People bodies are emulated as fully absorbing cylinders with a radius of 0.25m as per [JPK+13]. The reference scenario is built considering a total of 2000 samples for the training phase considering in an empty environment.
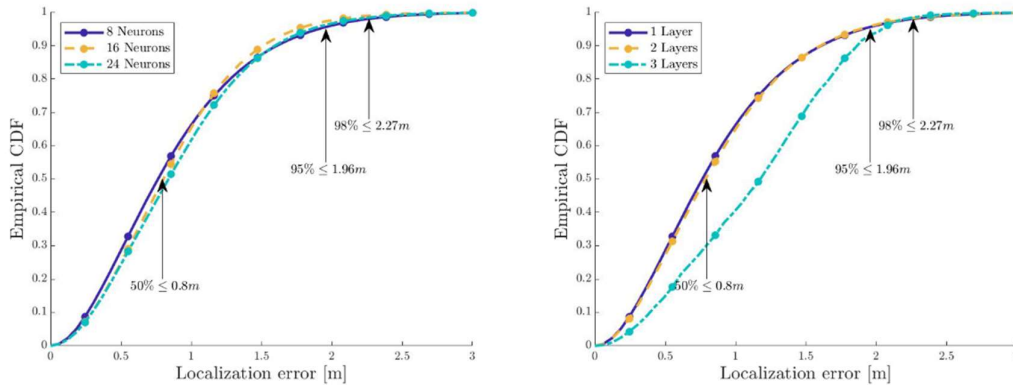
Figure 6-10: Cumulative Distribution Function of the intruder localization error.

Figure 6-10 shows on the left-hand side the intruder localisation performance with 1 hidden layer network with different number of neurons, while on the right-hand side it shows the locali-sation performance achieved by keeping the hidden layer size at 8-neurons and changing the depth of the network. The obtained results show that it is possible to achieve a localisation accuracy slightly above 2 meters in 98% of the cases.

7 Spectrum sensing, RF mapping and fingerprinting localisation

The purpose of this section is to provide a brief overview of the principles of radio localisation based on wireless fingerprinting via spectrum sensing and RF mapping. Then the general use of RISs in this context will be detailed, followed by a description of the contributions developed within the RISE-6G project.

7.1 Motivations and challenges

Among all the localisation technologies, wireless fingerprinting localisation (WFL) represents an effective technique due to its simplicity and deployment practicability [VDH+07], [DCP+17], [NGG+21]. WFL avoids hardware deployment cost and effort by relying on existing network infrastructure such as WiFi or cellular networks, and it works in two phases: an offline training phase and an online localisation phase. During the training phase, RF measurements (also known as fingerprints) at known locations are collected in a database. The fingerprint database is also referred to as the RF map. During the online phase, users' position is determined by comparing the real-time RF measurement with the entries in the database. Typically, WFL ex-ploits received signal strength indicator (RSSI) as the RF measurement due to its availability at both the transmitter and receiver sides.

Although WFL is one of the most exploited techniques in localisation, there remains a lot of unsolved research problems, mainly related to the accuracy of the RF map and the availability of data. The RF map database can be obtained/generated by different methods. For traditional fingerprinting, a measurement campaign must be carried out over a grid of L candidate loca-tions, collecting K RSSI values for each position. However, obtaining the full radio map of an area is time consuming and labor intensive. To reduce the cost and effort of collecting a full radio map database, we can resort to estimation techniques that interpolate the RF map from a few collected measurements. In this case, we can distinguish between parametric and non-parametric estimation models. In the parametric case, since the aim is to model the propagation of the radio signal, a natural choice is the pathloss model, whose parameters (e.g., pathloss exponent, pathloss at reference point, etc.) are estimated from the collected measurements

[DCP+17]. Instead, in the non-parametric case, the RF map is generated probabilistically modelling RSSI measurements using, e.g., a Gaussian distribution [SY+15]. An optimization procedure is then applied to tune the hyperparameters of the non-parametric model, with the aim of predicting RSSI measurements at any arbitrary location. Finally, once the RF map has been created, the best location estimate of the user is selected using some minimum distance criterion in the signal space, e.g., minimum distance, k-nearest neighbours, etc.

In this context, the deployment of multiple RISs can improve the performance of WFL, thanks to the possibility to control the EM environments and generate easily differentiable RF maps, which represent the input of WFL estimators [NGG+21]. Furthermore, active RISs can also be helpful to collect further RSSI measurements over the area of interest, thus improving the performance of the RF mapping step.

7.2   Contributions from RISE-6G

In the following, we describe RISE-6G contribution for RIS-empowered WFL. We currently have a single contribution that proposes to build a set of RF maps using graph signal processing tools, with the aim of performing RIS-empowered WFL. An overview of the setup and system model is provided in Table 7-1.

Table 7-1 An overview of spectrum sensing, RF mapping and fingerprinting contributions

Architecture	Cont. #D-1: Graph-based Radio MAP Cartography for RIS-aided Fingerprinting Localisation
Nr BS	Multiple
Nr RIS	Multiple
Nr UEs	1
UE Mobility	Static
RIS Type	reflective / quasi-active
Setup	
Uplink/Downlink	DL
Indoor/outdoor/UAV	Indoor/outdoor
Frequency Band	Any
Narrowband/wideband	NB
Near field/far field	Far field
LOS/NLOS (BS-RIS-UE)	LOS/NLOS
Measurement type	Multiple RSSI
RIS configuration strategy	Fixed set of sounding RIS profiles
Who collects measurements	BS
Synchronisation	unsynchronized
Metric optimised	MSE for RF mapping; RMSE for localization

7.2.1   Contribution #D-1: Graph-based radio MAP cartography for RIS-aided fingerprinting localisation

Motivation and context

Wireless fingerprinting localisation (WFL) is performed exploiting readily available RSSI at the mobile device. Typically, in WFL applications, a dense spatial database of RSSI measurements (i.e., the fingerprints) is constructed during an offline phase usually along a grid of L locations. The standard approach towards enhancing WFL accuracy is to deploy multiple APs, thus improving the dimensionality of the fingerprint at the expense of added infrastructure, signal processing costs, and data collection burden. Recently, RISs have been exploited to flexibly alter

the RF map environment with the aim of performing WFL, replacing the requirement of multiple APs by improving the dimensionality and diversity of the wireless fingerprints [NGG+21]. However, the collection of fingerprints over the area of interest can be a heavy, time-consuming task, which can be tackled resorting to data augmentation methods from the collection of a subset of samples. In the sequel, we introduce a method for RF map cartography, which interpolates several RF maps (one for each fingerprint) from a subset of collected measurements, exploiting graph signal processing tools. The resulting maps are then used as input of the WFL algorithm to perform localisation of the mobile device using conventional criteria based on, e.g., minimum Euclidean distance, k-nearest neighbours, etc.

Methodology

The scenario comprises several BSs and RISs. To create a rich set of fingerprints for localisation, each BS switches among different transmission strategies (e.g., on-off, or changing the beamforming), and the RISs exploit different phases profiles. We assume K different APs/RISs configurations such that the fingerprints at every location are collected into a K-dimensional vector. Also, we consider the challenging case where we can observe the vector of K RSSI measurements only over a subset of the L locations. In such a case, active RISs can be used to measure RSSI at some points in the space, thus helping WFL not only in terms of fingerprints augmentation, but also for data collection.

To implement WFL in such a scenario, we need a data augmentation method that interpolates the K EM radio frequency maps over the points where we do not collect RSSI measurements. To this aim, we hinge on graph signal processing tools: Each of the L candidate locations are vertices of a graph, where the vector of K RSSI measurements in each spatial point represents the signal associated with the corresponding vertex. The edges of the graph represent data similarities, which depend on physical parameters such as, e.g., distance among nodes, shadowing effects, and AP/RIS transmission strategy. Here, we assume the graph is either unknown or only partially known, i.e., it represents a further variable of the problem. The idea is to leverage on the smoothness of the signal defined over such graph to enable efficient interpolation of missing data. To this aim, we devised an optimization criterion that learns the overall signal and the associated graph from the collected samples, with the aim of minimizing the fitting error properly penalized by a graph smoothness regularization factor. The resulting bi-convex problem is solved using an efficient successive convex approximation method (SCA) that is guaranteed to converge to a local solution of the problem. This interpolation method enables the cartography of K EM radio maps from a few collected samples and drives the following WFL. In particular, once the EM radio maps are estimated, WFL is readily obtained by RSSI measurement collected at the UE exploiting a conventional criterion such as, e.g., minimum distance or k-nearest neighbour.

Results and outcomes

We tested our algorithm using a RIS-path loss model over a specific geographic area in Rome, Italy. In such a scenario, there are two BSs and two RISs, which generate a total of six fingerprints. The scenario is illustrated in Figure 7-1 (left). For every fingerprint, we apply the previously described interpolation method, assuming a certain number of collected measurements over the field. Finally, we apply WFL with 4-nearest neighbours criterion. The results are illustrated in Figure 7-1 (right), where we show the behaviour of the localisation error with respect to the number of collected samples, for different values of additive noise power. As expected, from Figure 7-1 (right), localisation performance improve by increasing the number of collected measurements used for interpolation and, subsequently, for localisation.
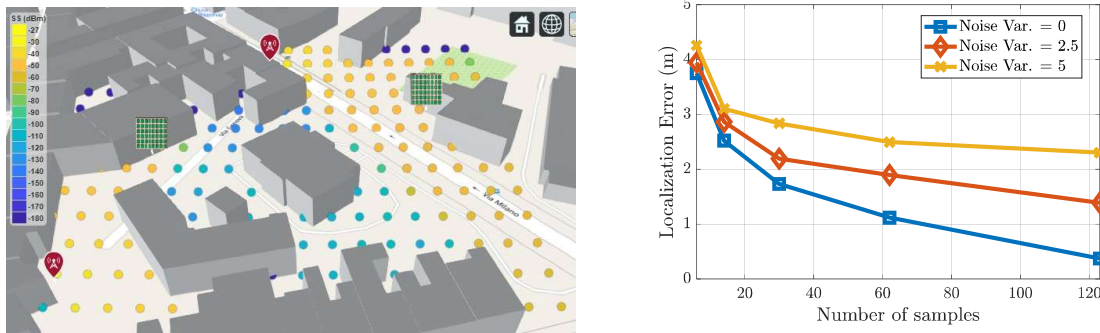
Figure 7-1: RIS-aided fingerprinting localisation. (Left) Considered scenario. (Right) Localisation error.

Perspective and relation to other WP5 contributions

Since this work proposes a general method for EM radio map interpolation, it can be used also in other WPs for spatial information-based resource allocation in order to, e.g., reduce EMF absorption in some specific regions while maximizing communication performance in other areas.

8 Relation to proof of concept demonstrations and feasibility

The table below summarizes the requirements on the WP7 PoC hardware from the WP5 perspective. Note that this table relates to D2.3 [RISED23] (Tables 6.3-6.7), but provides additional details.

It shall be understood that both BS and UE entities are herein intended in a very generic way, depending on the level of abstraction considered in each of the selected candidate demonstration scenarios reported below. The latter can for instance refer to a "close" commercial device, a semi-open test-oriented device (still fairly similar to a commercial device tough), a Software Defined Radio (SDR) transceiver or the receiving extremity of a channel sounding chain. Likewise, the so-called BS may represent a commercial access point, a SDR-based emulated BS or the transmitting extremity of a channel sounder.

As a basic concrete example, if a UE involved in field trials (besides one BS and one reflective RIS) could provide only Reference signal Receive Power (RSRP) values, but no IQ data, then one would mainly demonstrate RIS-enabled positioning based on signal strength measurements, thus offering limited capabilities in terms of post-porcessing and accordingly, in terms of high-resolution localisation capabilities. However, in the very example, one could still envision a simple demonstration scenario with 1 BS, 2 RIS and 1 UE, as follows:

- o The BS sends pilots towards each RIS;
- o Each RIS uses a sequence of directional beams. The 2 RIS would hence need to operate in a coordinated fashion;
- o The UE measures the RSRP and the RIS beams with maximum RSRP provide the direction;
- o The UE can then be localized based on the direction from 2 RIS (conceptually, as the intersection of 2 lines in 3D).

A more complete analysis regarding localisation feasibility depending on the target scenario, the deployment assumptions (regarding BS, RIS and UE), the extracted radio physical layer parameters, and the transmission settings, can also be found in [KDA+22].

Table 8-1. Hardware requirements of the WP5 methods

Method→	Localisation by AOD (estimated via RSS) from 2 RISs	Localisation by AOD (estimated via IQ samples) from 2 RISs	Localisation by AOD (estimated via IQ samples) and TOA from 1 RIS	Joint mobile UE localisation and velocity estimation in Near-Field from 1 RIS	Localisation by AOA (estimated via IQ samples) from 3 sensing RISs
Reference	N/A	N/A	N/A	Section 5.2.6	Section 5.2.5, [AVW22]
Main benefits from RIS (Vs. conventional non-RIS approaches)	-Positioning with **1 single active BS** out of SC DL transmissions -Positioning under **NLoS** (btw. UE and BS)	-Positioning with **1 single active BS** out of SC DL transmissions -Positioning under **NLoS** (btw. UE and BS)	Joint **positioning and synchronization** with **1 single active BS** out of MC DL transmissions	Joint **positioning and velocity** estimation with **1 single active BS** out of SC DL transmissions	**BS-free** UL positioning
UL or DL	DL	DL	DL	DL	UL
Carrier	mmWave preferred or sub-6GHz in clean environment	mmWave preferred or sub-6GHz in clean environment	mmWave	mmWave preferred or sub-6GHz in clean environment	mmWave
Bandwidth required	N/A	N/A	400 MHz	N/A	N/A
Indoor / outdoor	N/A	N/A	N/A	both	Both
Multi-antenna BS	No	No	No	No	No
Multi-antenna UE	No	No	No	No	No
LOS from BS to UE required	No	No	Yes	No	N/A (No BS but LoS required from EU to RIS)
Number of UEs, RISs, BSs needed	1 UE, 1 BS, 2 RIS (Reflect mode)	1 UE, 1 BS, 2 RIS (Reflect mode)	1 UE, 1 BS, 1 RIS (Reflect mode)	1 UE, 1 BS, 1 RIS (Reflect mode)	1 UE, at least 2 RIS (Rx mode)
Need for IQ samples at UE or BS (or at RIS)	No	Yes (at UE)	Yes (at UE)	Yes (at UE)	Yes (at RIS)
Need for RSS measurements at UE or BS	Yes, RSS per beam	Yes	Yes	Yes	No
Need for knowledge of complex 3D beampatterns at BS, RIS or UE	No	Yes	Yes	Yes	No
Need of knowledge of RIS element response a(theta) and RIS phase configuration	No	Yes	Yes	Yes	Yes
Needs several random RIS configurations	No	Yes	Yes	Yes	No
Needs (DFT) RIS beams	Yes	Yes	Yes	Yes	Yes
Feedback channel for RIS control	Only for timing of RIS configuration	Only for timing of RIS configuration	Only for timing of RIS configuration	Only for timing of RIS configuration	Yes
Synchronization requirement	Global knowledge of start and end of transmissions,	Global knowledge of start and end of transmissions,	Global knowledge of start and end of transmissions,	Global knowledge of start and end of transmissions,	Global knowledge of start and end of

	start and end of each RIS configuration.	start and end of each RIS configuration.	start and end of each RIS configuration.	start and end of each RIS configuration.	transmissions, start and end of each RIS configuration. Synchronization of measurements sent from each RIS to central controller.
Update rate of RIS configuration	Arbitrary, provided UE is static	Arbitrary, provided UE is static	Arbitrary, provided UE is static	Arbitrary, provided UE is static	Arbitrary, provided UE is static.
Transmission duration	Should be sufficient to measure RSS per RIS configuration	In principle 1 symbol per RIS configuration is sufficient	In principle 1 OFDM symbol per RIS configuration is sufficient	In principle 1 symbol per RIS configuration is sufficient	In principle 1 symbol per RIS configuration is sufficient.
Transmission waveform parameters	Arbitrary pilot signal	Arbitrary pilot signal	Unit-modulus data (in frequency domain)	Arbitrary pilot signal	Arbitrary pilot signal
Other UE requirements	Should provide RSS per RIS configuration, and AOD per RIS configuration	Should provide IQ samples per RIS configuration.	Should provide IQ samples per RIS configuration.	Should provide IQ samples per RIS configuration. UE should be close to the RIS.	Should provide IQ samples per RIS configuration.
Other BS requirements	N/A	N/A	N/A	N/A	N/A
Other RIS requirements	Many successive RIS configurations needed	Many successive RIS configurations needed	Many successive RIS configurations needed	Many successive RIS configurations needed	Many successive RIS configurations needed

9   Conclusions

RISs have a great potential to control the radio wave propagation and geometry of multipath-aided localisation problems, thus enabling highly accurate localization and sensing, radio-frequency mapping and obstacles/activity detection. Due to the unique properties of RISs, those functionalities can be achieved with reduced, and in some cases even without reliance on BSs, making them particularly suitable in scenarios where conventional architectures and deployments fail. However, the introduction of RIS constitutes a shift of paradigm that calls for new techniques and algorithms.

This deliverable addresses that need by outlining several novel RIS-based channel estimation, localisation and sensing algorithms in a wide range of scenarios. The document and contributions presented therein constitute an intermediary specification from WP5 to the RISE-6G project.

References

[3GPP10]	"Physical channels and modulation, release 16, V16.2.0," 3GPP, Sophia Antipolis, France, Rep. 3GPP TS 36.211, Mar. 2010.
[ASA+21]	G. C. Alexandropoulos, N. Shlezinger, I. Alamzadeh, M. F. Imani, H. Zhang, and Y. C. Eldar, "Hybrid reconfigurable intelligent metasurfaces: Enabling simultaneous tunable reflections and sensing for 6G wireless communications," [Online] https://arxiv.org/pdf/2104.04690.pdf, 2021.
[AV20]	G. C. Alexandropoulos and E. Vlachos, "A hardware architecture for reconfigurable intelligent surfaces with minimal active elements for explicit channel estimation," in *Proc. IEEE International Conference on Acoustics, Speech, and Signal Processing*, Barcelona, pp. 9175–9179, Spain, 4–8 May 2020.

[AVW22]	G. C. Alexandropoulos, I. Vinieratou and H. Wymeersch, "Localisation via Multiple Reconfigurable Intelligent Surfaces Equipped With Single Receive RF Chains," in *IEEE Wireless Communications Letters*, vol. 11, no. 5, pp. 1072-1076, May 2022.
[AZW+20]	S. Abeywickrama, R. Zhang, Q. Wu, and C. Yuen, "Intelligent reflecting surface: Practical phase shift model and beamforming optimization," *IEEE Transactions on Communications*, vol. 68, no. 9, pp. 5849–5863, 2020.
[BG06]	M. Biguesh, A.B. Gershman, "Training-based MIMO channel estimation: a study of estimator tradeoffs and optimal training signals," *IEEE Transactions on Signal Processing*, vol. 54, no. 3, pp. 884-893, 2006.
[BSY19]	F. Bellili, F. Sohrabi, W. Yu, "Generalized approximate message passing for massive MIMO mmWave channel estimation with Laplacian prior," *IEEE Transactions on Communications*, vol. 67, no. 5, pp. 3205-3219, 2019.
[CJG+22]	H. Chen, F. Jiang, Y. Ge, H. Kim, H. Wymeersch,"Doppler-Enabled Single-Antenna Localisation and Mapping Without Synchronization", pre-print available on Arxiv: https://arxiv.org/abs/2205.15427
[CKA+20]	G. K. Carvajal, M. F. Keskin, C. Aydogdu, O. Eriksson, H. Herbertsson, H. Hellsten, E. Nilsson, M. Rydström, K. Vänas, and H. Wymeersch. "Comparison of automotive FMCW and OFDM radar under interference," in 2020 IEEE Radar Conference (RadarConf20), 2020, pp. 1–6
[DCP+17]	Yiu, S., Dashti, M., Claussen, H., & Perez-Cruz, F. (2017). Wireless RSSI fingerprinting localisation. Signal Processing, 131, 235-244.
[DNA+20]	D. Dardari, D. Nicoló, G. Anna, and G. Francesco. "LOS/NLOS Near-Field Localisation with a Large Reconfigurable Intelligent Surface." IEEE Transactions on Wireless Communications (2021).
[DSF+20]	F. Devoti, V. Sciancalepore, I. Filippini, and X. Costa-Perez, "Pasid: Exploiting indoor mmwave deployments for passive intrusion detection," in IEEE INFOCOM 2020-IEEE Conference on Computer Communications. IEEE, 2020, pp. 1479–1488.
[FSD+17]	I. Filippini, V. Sciancalepore, F. Devoti, and A. Capone, "Fast cell discovery in mm-wave 5g networks with context information," IEEE Transactions on Mobile Computing, vol. 17, no. 7, pp. 1538–1552, 2017.
[JPK+13]	M. Jacob, S. Priebe, T. Kurner, M. Peter, M. Wisotzki, R. Felbecker, and W. Keusgen, "Fundamental analyses of 60Ghz human blockage," in 2013 7th European Conference on Antennas and Propagation (EuCAP). IEEE, 2013, pp. 117–121.
[KDA+22]	K. Keykhosravi, B.Denis, G.C. Alexandropoulos, A. Albanese, V. Sciancalepore, S. He, H. Wymeersch, "Leveraging RIS-Enabled Smart Signal Propagation for Solving Infeasible Localisation Problems", arXiv preprint arXiv:2204.11538, Avril 2022.
[KKD+21]	K. Keykhosravi, M. F. Keskin, S. Dwivedi, G. Seco-Granados, and H. Wymeersch, "Semi-passive 3D positioning of multiple RIS-enabled users," *IEEE Transactions on Vehicular Technology*, vol. 70, no. 10, pp. 11073-11077, Oct. 2021.
[KKS+21]	K. Keykhosravi, M. F. Keskin, G. Seco-Granados, and H. Wymeersch, "SISO RIS-enabled joint 3D downlink localization and synchronization," Proc. IEEE ICC'21, June 2021.
[KKS+22]	K. Keykhosravi, F. Keskin, G. Seco-Granados, P. Popovski, and H. Wymeersch, "RIS-Enabled SISO Localisation under User Mobility and Spatial-Wideband Effects," *IEEE Journal of Selected Topics in Signal Processing*, 2022, accepted.
[KSA+22]	K. Keykhosravi, G. Seco-Granados, G. C. Alexandropoulos, and H. Wymeersch, "RIS-Enabled Self-Localisation: Leveraging Controllable Reflections with Zero Access Points," in *Proceedings of IEEE International Conference on Communications*, Seoul, South Korea, 16–20 May 2022.
[LLH+16]	J.-J. Lin, Y.-P. Li, W.-C. Hsu, and T.-S. Lee, "Design of an FMCW radar baseband signal processing system for automotive application," SpringerPlus, vol. 5, 12 2016.

[NGG+21]	Nguyen, C. L., Georgiou, O., Gradoni, G., & Di Renzo, M. (2021). Wireless Fingerprinting Localisation in Smart Environments Using Reconfigurable Intelligent Surfaces. *IEEE Access*, *9*, 135526-135541.
[OKW+22]	C. Ozturk, M. F. Keskin, H. Wymeersch, and S. Gezici, "RIS-aided Near-Field Localisation under Phase-Dependent Amplitude Variations," *IEEE Transactions on Wireless Communications*, 2022, under review.
[PRL+18]	J. A. del Peral-Rosado, R. Raulefs, J. A. LÃspez-Salcedo, and G. Seco-Granados, "Survey of cellular mobile radio localisation methods: From 1G to 5G," IEEE Commun. Surveys Tuts., vol. 20, no. 2, pp. 1124– 1148, 2018.
[RDK+21]	M. Rahal, B. Denis, K. Keykhosravi, B. Uguen, H. Wymeersch, "RIS-Enabled Localisation Continuity Under Near-Field Conditions", Proc. IEEE SPAWC'21, Sept. 2021. Pre-print available on ArXiv: https://arxiv.org/abs/2109.11965
[RDK+22a]	M. Rahal, B. Denis, K. Keykhosravi, M.F. Keskin, B. Uguen, H. Wymeersch, "Nearfield Localisation-Optimal RIS Profile Design and Practical Time Sharing", IEEE VTC 2022 – Spring, Workshop on Localisation and Sensing with Intelligent Surfaces for 6G Networks, Helsinki, June 2022. Pre-print available on ArXiv: http://arxiv.org/abs/2203.07269
[RDK+22b]	M. Rahal, B. Denis, K. Keykhosravi, M.F. Keskin, B. Uguen, G.C. Alexandropoulos, H. Wymeersch, "Arbitrary Beam Pattern Approximation via RISs with Measured Element Responses", EuCNC'22 & 6G Summit'22, June 2022. Pre-print available on ArXiv: http://arxiv.org/abs/2203.07225
[RHD14]	F. Roemer, M. Haardt, & G. Del Galdo, "Analytical performance assessment of multi-dimensional matrix-and tensor-based ESPRIT-type algorithms," *IEEE Transactions on Signal Processing*, vol. 62, no. 10, pp. 2611-2625, 2014.
[RISED23]	M. Crozzoli, et al. "Reference System, Scenarios and Use Cases Analysis: Final Results", Deliverable D2.3 of the RISE-6G Project, Feb. 2022
[RISED24]	V. Sciancalepore et al., ''Metrics and KPIs for RISE Wireless Systems Analysis: First Results", Deliverable D2.4 of the RISE-6G Project, Feb. 2022
[RISED51]	H. Wymeersch et al., ''Control for RIS-based Localisation and Sensing (Intermediary Specifications)", Deliverable D5.1 of the RISE-6G Project, April 2022
[SFS+18]	Y. Sun, T. Fei, F. Schliep, and N. Pohl, "Gesture classification with handcrafted micro-Doppler features using a FMCW radar," in 2018 IEEE MTT-S International Conference on Microwaves for Intelligent Mobility (ICMIM), Munich, Germany, Apr. 2018
[SGD+17]	A. Shahmansoori, G. E. Garcia, G. Destino, G. Seco-Granados, H. Wymeersch, "Position and orientation estimation through millimeter-wave MIMO in 5G systems," *IEEE Transactions on Wireless Communications*, vol. 17, no. 3, pp. 1822-1835, 2017.
[SY+15]	Yiu, Simon, and Kai Yang. "Gaussian process assisted fingerprinting localisation." *IEEE Internet of Things Journal* 3.5 (2015): 683-690.
[TLR04]	R. S. Thomä, M. Landmann, A. Richter, "RIMAX—A maximum likelihood framework for parameter estimation in multidimensional channel sounding," in *Proceedings of the International Symposium on Antennas and Propagation (ISAP'04)* pp. 53-56, 2004.
[VDH+07]	Varshavsky, A., De Lara, E., Hightower, J., LaMarca, A., & Otsason, V. (2007). GSM indoor localisation. *Pervasive and mobile computing*, *3*(6), 698-720.
[WHD+20]	H. Wymeersch, J. He, B. Denis, A. Clemente, and M. Juntti, "Radio localisation and mapping with reconfigurable intelligent surfaces: Challenges, opportunities, and research directions," IEEE Veh. Technol. Mag., vol. 15, no. 4, pp. 52–61, Dec. 2020.
[WLW+18]	Wen, F., Liu, P., Wei, H., Zhang, Y., & Qiu, R. C. (2018). Joint azimuth, elevation, and delay estimation for 3-D indoor localisation. *IEEE Transactions on Vehicular Technology*, *67*(5), 4248-4261.
[WSD+21]	Wymeersch, H., Shrestha, D., De Lima, C. M., Yajnanarayana, V., Richerzhagen, B., Keskin, M. F., ... & Parkvall, S. (2021, September). Integration of communication and sensing in 6g: a joint industrial and academic perspective. In *2021 IEEE 32nd Annual International Symposium on Personal, Indoor and Mobile Radio Communications (PIMRC)* (pp. 1-7). IEEE.
[WWS+17]	X. Wu, C.-X. Wang, J. Sun, J. Huang, R. Feng, Y. Yang, and X. Ge, "60-ghz millimeter-wave channel measurements

	and modeling for indoor office environments," IEEE Transactions on Antennas and Propagation, vol. 65, no. 4, pp. 1912–1924, 2017
[ZGL19]	Zafari, F., Gkelias, A., & Leung, K. K. (2019). A survey of indoor localisation systems and technologies. *IEEE Communications Surveys & Tutorials, 21*(3), 2568-2599.